Title

Structural and comparative analysis of GLUT1 and GLUT3 and transport regulation in the Sugar Porter family

Authors

Tânia Filipa Custódio[1*], Peter Aasted Paulsen[1*], Bjørn Panyella Pedersen[1,2#]

1) Department of Molecular Biology and Genetics, Aarhus University, Gustav Wieds Vej 10, DK-8000 Aarhus C, Denmark.

2) Aarhus Institute of Advanced Studies, Aarhus University, Høegh-Guldbergs Gade 6B, DK-8000 Aarhus C, Denmark.

* Contributed equally

Corresponding author. E-mail: bpp@mbg.au.dk

Abstract

The human glucose transporters GLUT1 and GLUT3 are canonical members of the Sugar Porter (SP) family and central for uptake of glucose. GLUT1 and GLUT3 share a fully conserved substrate-binding site with identical substrate coordination, but differ significantly in transport affinity in accordance with their physiological function. Here we present a 2.4 Å crystal structure of GLUT1 and make a direct comparison between GLUT1 and GLUT3 using both structural and functional data. Our work shows that interactions between a cytosolic Sugar Porter motif and a conserved "A motif" stabilize the outward conformational state and increases substrate affinity, while a previously undescribed Cl^- ion site and endofacial lipid/glucose binding site impede this interaction to modulate GLUT kinetics. The results provide an explanation for the difference between GLUT1 and GLUT3 glucose affinity, imply a general model for kinetic regulation in GLUTs and suggest a physiological function of the defining SP sequence motif in the Sugar Porter family.

Keywords

glucose transport, GLUT1, GLUT3, crystallography, A motif, SP motif, transport kinetics, Sugar Porter family, Major Facilitator superfamily

Introduction

In humans, GLUT proteins are responsible for cellular uptake of glucose. Basal cellular glucose uptake is mediated by GLUT1 (Mueckler et al., 1985), while GLUT3 is highly and specifically expressed in neurons and other tissues with high energy demand (Simpson et al., 2008). In line with its physiological role, GLUT3 has been shown to have higher glucose affinity (~3 mM) than GLUT1 (~10-20 mM) (Burant and Bell, 1992; Nishimura et al., 1993; Maher, Davies-Hill and Simpson, 1996; Bentley et al., 2012; De Zutter et al., 2013); however this difference in affinity cannot readily be explained by the glucose binding site of the two proteins, which is highly conserved and structurally identical (Deng et al., 2014, 2015).

GLUTs belong to the Sugar Porter (SP) family, found in all kingdoms of life (Baldwin, 1993), and the largest branch of the Major Facilitator Superfamily (MFS). MFS proteins all share a common fold comprising 12 transmembrane helices (M1-M12) with a two-fold pseudo-symmetry between the N-domain (M1-6) and the C-domain (M7-12), and are defined by a signature motif, the "A motif", in the form of Gx_3[D/E][R/K]xGx[R/K][K/R] (Pao et al., 1998). Due to the inherent pseudo-symmetry of the superfamily, the A motif is found twice, located in the N-domain in the cytosolic loop connecting M2 and M3 and in the C-domain in the cytosolic loop connecting M8 and M9. The A motif is believed to be a key determinant of transport kinetics (Viitanen et al., 2013; Nomura et al., 2015; Zhang et al., 2015; Cain et al., 2000), and it may also modulate transport by direct lipid interactions (Martens et al., 2018). In addition to the A-motif, the Sugar Porter family also have a family-defining "Sugar Porter (SP) motif" located, also in duplicate, on both the cytosolic side in the N-domain directly after M6 and in the C-domain directly after M12. The SP motif takes the form of PESPR and PET[K/R]G in these two locations in GLUT proteins (Baldwin, 1993). The importance of SP motifs have been demonstrated through mutational studies, and is highlighted by their strong conservation in the SP family (Seyfang and Landfear, 2000; Sun et al., 2012); however, a functional role has not been established (Fig S1).

All SP proteins alternate between inward facing and outward facing conformations with respect to the central substrate binding site, and the transition between these two states define sugar transport (Fig 1A). When the transporter is in the outward facing conformation (C_{out}), extracellular sugar will bind to the central binding site ($C_{out}S$), and be transported to the inside ($C_{in}S$) as dictated by the concentration gradient across the membrane. The following conformational transition from the substrate-free inward conformation (C_{in}) to the substrate-free outward conformation (C_{out}) is needed to reset the transporter, and has been experimentally shown to be the rate-limiting step in GLUTs, consistent with thermodynamic models (Lowe and Walmsley, 1986; Wheeler and Whelan, 1988; Zhang and Han, 2016). During transport, the A motif has been found to control the degree of stabilization of the outward conformation (Jiang D et al., 2013; Zhang et al., 2015).

GLUT1 and GLUT3 provide a strong model system for understanding GLUT and SP protein kinetics, given their different kinetic properties despite identical substrate-binding pockets. However, few stud-

ies have directly compared the determinants of GLUT1 and GLUT3 kinetics (Burant and Bell, 1992; Maher, Davies-Hill and Simpson, 1996). Large variations between published studies can be attributed to the type of assay and substrate used to measure transport (Maher, Davies-Hill and Simpson, 1996). It is also important to consider the lipid environment, as GLUT proteins are highly sensitive to the lipid composition (Wheeler, Cole and Hauck, 1998; Hresko et al., 2016). A comparative study of the two proteins requires identical experimental setups as well as high-resolution structural information. To this end, we report a 2.4 Å resolution structure of human GLUT1 that reveals two previously unknown features: an intracellular glucose and/or lipid-binding site at the SP motif, and a chloride-ion binding site between the SP and A motifs. We present a direct one-to-one biochemical comparison between GLUT1 and GLUT3 in an identical experimental setup and examine and revalidate the differences between the two proteins. Based on the structural data, we pinpoint key elements of the cytosolic domain that modulate the kinetics of transport. These elements reside within the A and SP motifs of the N- and the C-domain and they provide a functional framework to better understand the role of these motifs in all SP and MFS proteins. The results provide a model that explains kinetic differences between GLUT1 and GLUT3, and furthermore suggest transport regulation by a structural framework found in the SP motif that can interact with lipids and/or intracellular sugar. We confirm this new model by mutational analysis and identify a single point mutation in the SP motif that can convert GLUT1 into a transporter with GLUT3-like kinetics and vice-versa.

RESULTS

Affinity and selectivity comparison between GLUT1 and GLUT3

In order to directly compare the kinetics of human GLUT1 and GLUT3 we expressed both proteins in *Xenopus* oocytes and measured uptake of 2-deoxyglucose (2-DG). Xenopus oocytes expressing GLUT1 or GLUT3 show a similar increase in 2-DG accumulation, while water-injected oocytes show that 2-DG uptake from endogenous transporters in the oocyte membrane is negligible (Fig 1B). Michaelis-Menten analysis of substrate saturation kinetics with GLUT1 resulted in a Km for 2-DG uptake of 9.5 mM (Fig 1C), comparable with previous reports in the literature (Burant and Bell, 1992; Bentley et al., 2012). The uptake was inhibited by the GLUT inhibitor cytochalasin B. GLUT3 displays a similar cytochalasin B-dependent behavior with a Km of 2.6 mM (Fig 1D). This is close to the values measured in rat primary cerebral granule neurons previously (Maher, Davies-Hill and Simpson, 1996). The protein levels of GLUT1 and GLUT3 in the oocyte membranes were detected by western blot using an engineered and identical epitope (derived form GLUT1) on both proteins, to allow direct comparison. The result shows that expression levels are comparable (Fig S2A) and kinetic parameters of GLUT3 are not affected by the introduced epitope (Fig S2B). We estimate the Vmax of GLUT1 to be 4920 pmol/oocyte/30min, and for GLUT3 to be 2-fold lower at Vmax 2537 pmol/oocyte/30min. Notably, in contrast to a study that calculated a higher turnover for GLUT3

compared to GLUT1 (Maher, Davies-Hill and Simpson, 1996), our results support another study that GLUT3 has a lower turnover than GLUT1 (De Zutter et al., 2013).

Substrate selectivity of both GLUT1 and GLUT3 was screened in an identical setup with a competition assay. For both transporters, glucose and mannose competed strongly with 2-DG (Fig 1E and F). Other sugars also competed for uptake but to a lesser extent, in accordance with previous literature (Burant and Bell, 1992; Deng et al., 2015). The similarities in selectivity are consistent with the structural conservation of the two substrate binding-sites and reinforce the idea that other regions of the transporters must be responsible for conferring the observed difference in substrate affinity and transport capacity found between GLUT1 and GLUT3.

The GLUT1 structure reveals new ligands

We subsequently solved the crystal structure of human GLUT1 to 2.4 Å resolution (Rfree 22.9%) (Table S1 and Fig S3-S4). The overall structure adopts an inward-open conformation that is almost identical to the 3.2 Å model published previously ($RMSD_{(CA)}$ 0.4 Å) (Fig S5A) (Deng et al., 2014). The authenticity of the earlier GLUT1 model has been questioned, owing to the presence of two stabilizing mutations in the studied protein. However, our crystal structure of native GLUT1 shows that the effect of these mutations is minimal. The structure contains residues 9-455 (of 492 residues total) and presents the canonical N-domain, the cytosolic ICH domain (ICH1-ICH4) and C-domain (Fig 2A). The high quality of the electron density map, compared to earlier studies, allows for the identification of several new ligands and 13 water molecules in the structure, as well as well-defined side chains (Fig S4). Crystals were grown in the presence of glucose and the detergent Nonyl-β-D-Glucoside (NG), which has a glucose head-group. In our maps, we clearly observe an NG molecule in the central sugar-binding site (Fig 2A and B and Fig S3-S4), despite having a 6-fold molar excess of glucose present (40 mM vs 6.5 mM). The entirety of the NG density is well defined and we can unambiguously model the hydrophobic tail as well as the headgroup moiety. There is less density for the tail, which could reflect flexibility or that the central binding site is occupied by a mixture of NG and glucose. Occupancy refinement using a mixed ligand model yields a reproducible 40/60% ratio between glucose and NG. As a conservative measure, the final model was built with only NG. Only residues from the C-terminal domain are part of the glucose headgroup coordination: seven polar interactions are established through residues from M7, M8 and M10. The D-glucopyranoside C2 and C4 hydroxyl groups are each coordinated by a single hydrogen bond from Gln282 and Asn288, respectively, while the C3 hydroxyl is coordinated by two hydrogen bonds with Asn288 and Gln283. The C6-OH forms three hydrogen bonds with the Glu380 and Asn317 residues. Furthermore, several hydrophobic residues including Gly384, Phe379 and Phe291 surround the D-glucopyranoside (Fig 2B). When compared with the binding of glucose in the 1.5 Å GLUT3 structure (Deng et al., 2015), we confirm that the atomic interactions are structurally identical and conserved between the two proteins (Fig S5B).

Next to the glucose headgroup, we observe an additional tubular density close to the binding site that fits with a PEG molecule, derived from the experimental setup (Fig 2A and B and Fig S4 and S5). This PEG molecule binds through interactions with Trp388, Trp412, Ile404, Thr137 and Ser80 (Fig S6A) and overlaps with the position of two inhibitors previously described, while it differs from that of the cytochalasin B binding site, despite a partial spatial overlap (Fig S6B) (Kapoor et al 2016).

Ligand interaction with the SP motifs

When superposed, the structures of both the A and SP motifs are highly similar between the N- and C-domains of GLUT1 and GLUT3 ($RMSD_{(CA)}$ <0.8 Å) (Fig S7A-C). In our GLUT1 structure, the two SP motifs are located directly below the two A motifs (Fig 2C and D). Part of the C-domain SP motif is disordered, while the N-domain SP motif is visible in the electron density and has its residues moved away from the A motif to interact with ligands.

We observe an additional strong density on the cytosolic side of GLUT1 interacting with the N-domain SP motif. The main part of this density matches a glucose, but at a lower density threshold additional density appears that fits an aliphatic tail, and in analogy with our modeling for the central binding site, we therefore modeled this as an NG molecule (Fig 3A and Fig S4). In a physiological context, this could be a potential allosteric binding site, regulated by either a lipid headgroup and/or a substrate molecule. The D-glucopyranoside headgroup in this "secondary site" establishes polar interactions with Arg93, Asn94, Glu209, Arg218, and Arg223 from both the N-domain SP motif, ICH1-2 and M3 residues (Fig 3A). The headgroup thus support the charged network of the conserved cytosolic residues, which in turn moves the SP motif residues away from the A motif residues and stabilize the inward-open conformation of GLUT1. This secondary site is not observed in the 1.5 Å structure of GLUT3 in the outward conformation despite this being a glucose-bound form (50 mM glucose and no NG present). The sequences are identical between GLUT1 and GLUT3 for these interacting residues, except a single residue, Arg223 in GLUT1 (Fig S1). To evaluate whether the secondary site density was derived from the experimental setup, we analyzed the previously published 3.2 Å GLUT1 dataset (Deng et al., 2014), where we also observe a clear density in the map at this site.

Another unexpected density feature was also prevalent in our map. There was a very strong spherical density (9.1 sigma peak) between the SP motif and the A motif of the N-domain, that could not be explained by a water molecule. The coordinating atoms indicates a negatively charged species such as a chloride ion, so we devised a follow-up experiment exploiting the strong anomalous scattering from the chloride chemical congener bromide. By replacing Cl^- with Br^- in the crystal it is possible to search for anomalous density peaks to identify bromide ion positions which will reveal the position of chloride in the original dataset (Ekberg et al., 2010). This experiment lead to a single strong anomalous peak (7.3 sigma) at the position of the spherical density, allowing us to unambiguously

identify this peak as a Cl^- ion (Fig 3B) positioned between the SP and A motif in the N-domain. This is the first time a chloride binding site has been identified in the SP family.

Identifying residues that influence the kinetics of GLUT1 and GLUT3

To pinpoint residues that control kinetic properties of GLUT1 and GLUT3, we initially focused on residues of the cytosolic ICH domain. Several known disease mutants cluster at the A motif, SP motif and in the ICH domain in general (Sun et al. 2012). For instance, Arg223Pro/Gln are two disease mutants that lead to GLUT1-Deficiency Syndrome by reducing cellular glucose uptake (Suls et al., 2009; Lee et al., 2014). In our structure, Arg223 is part of the interaction interface of the secondary site . In addition, Arg223 is the only residue that differs between GLUT1 and GLUT3 that directly interacts with the NG/glucose found there, suggesting that this residue could be implicated in isoform-specific differences mediated by substrate regulation. We made both disease mutants, R223P, R223Q, as well as the GLUT1 to GLUT3 isoform mutant R223N and tested them in our oocyte uptake assay. 2-DG uptake for R223N revealed only a moderate increase in substrate affinity. The Km value changed from the wild-type 9.5 mM to 7.5 mM (Fig 3C). Similarly, the R223P mutant that should mimic GLUT1-deficiency syndrome gave a Km of 7.2 mM. Neither of these changes are significant and we speculate that the R223P disease phenotype is not directly related to glucose transport. Substrate affinity for the GLUT1- deficiency syndrome R223Q mutant was also analyzed and revealed a 2.5-fold reduction of substrate affinity, giving a Km value of 24 mM (Fig 3D). This observed reduction in affinity would fit with the disease phenotype in this case. For all the three mutants, the substrate uptake rates do not appear to be affected and expression levels were found to be equal or higher than the WT protein (Fig. S8).

The role of the SP motif

The identification of the chloride binding site highlight a key change between inward- and outward conformation found in the SP motif. Here, the essential glutamate residue interacts with the A motif in the outward conformation, but flips out and away from the A motif in the inward conformation. Expanding to other Sugar Porter structures available, a consistent picture emerge: All structurally characterized members of the SP family show a well-defined and precisely-positioned conformation for the sugar porter glutamate residue (E209 and E454 in GLUT1) (Fig S9). In the outward-facing conformation, the equivalent glutamate residue of the SP motif of human GLUT3 (Deng et al., 2015), rat GLUT5 (Nomura et al., 2015) and the *Arabidopsis* proton symporter STP10 (Paulsen, Custódio and Pedersen, 2019) interacts with the A motif, establishing hydrogen bonds with amide groups of the last 2 residues (R92 and R93 in GLUT1) of the A motif (Fig S9A). We name this interaction network, found only in outward conformations of SP proteins, the "SP-A network". In our inward-facing conformation of the human GLUT1, as well as the bovine GLUT5 (Nomura et al., 2015) and the

bacterial sugar/proton symporters XylE (Sun et al., 2012) and GlcPse (Iancu et al., 2013), the glutamate residue is pointing away from the A motif, towards the cytosol (Fig S9B).
The position of the acid group of the glutamate in the SP-A network is replaced by the identified Cl^- ion in the GLUT1 structure (Fig 4A). This suggests a hypothesis where the glutamate residue in the SP-A network competes with a Cl^- ion for interaction with the A motif, while the glutamate interaction to the A domain stabilizes the outward conformation. We set forth to investigate this by removing the acid group of the relevant glutamates of both GLUT1 (E209Q) and GLUT3 (E207Q) (Fig 4). By this hypothesis, these mutants are predicted to weaken the interaction with the A motif in the outward conformation and fail to compete with the Cl^- ion. As a result, the outward-facing conformation should be disfavored and transport affinity should decrease, as the protein will stabilize in the inward conformation. Our hypothesis was supported by both of these mutations. Oocyte uptake revealed a reduced 2-DG uptake due to a ~2-fold decrease in the binding affinity compared to the wild-type protein (Fig 4B and C). According with our model, V_{max} values, which can be defined as the frequency of the interconversion between the outward and the inward conformations, should decrease. This effect can be seen for the GLUT3 (E207) mutant but not for the GLUT1 (E209Q) mutant. However, protein expression levels appear to be higher for the mutants compared to WT proteins (Fig S8), restricting our analysis.

The C-domain SP-A network is less well defined. Nevertheless, we investigated the two C-domain SP-A network glutamates of both GLUT1 and GLUT3 by changing them to glutamines (Fig 5) (E454Q (GLUT1) and E452Q (GLUT3)). Uptake revealed a reduced 2-DG uptake in the GLUT3 E452Q mutant and similar rates, but surprisingly, for the GLUT1 E454Q mutant, the Km value increased to 6 mM and a 2-fold decrease in the V_{max} (Fig 5B and C). This puzzling result made us refocus on the one residue of the C domain SP motif that is different between GLUT1 and GLUT3: Lysine 456 in GLUT1 that is an Arginine (R454) in GLUT3 (Fig 5A).
In the outward facing GLUT3 structure, Arg454 is part of the SP-A network to the A motif together with Glu452 (Fig 5A). The lysine residue is not resolved in the GLUT1 structures, but in the inward conformation of the GLUT1 bacterial homologue XylE, the equivalent residue is establishing a salt bridge with an acidic residue from the A motif (Fig S10). We hypothesized that only the arginine is able to bind to the A motif in the outward conformation, leading to a stabilization of the outward conformation for GLUT3 compared to GLUT1. Based on this model, the very mild mutant GLUT1 K456R should improve substrate affinity by mimicking the GLUT3 isoform and destabilize the inward conformation via a favorization of the SP-A network. We tested this mutant and the K_m values changed to a 2-fold higher affinity (4.2 mM) and 2.5-fold decrease in V_{max}, very similar to that of native GLUT3, in support of the model (Fig 5D). To further confirm the hypothesis, the inverted mutation was made on GLUT3, R454K. The transport affinity of the mutant was strongly affected with a 6-fold lower affinity than native GLUT3, (K_m 17 mM) (Fig 5E), again supporting this model.

Protein expression levels were found to be equal or higher than the WT protein for all the C-terminal mutants (Fig S8).

DISCUSSION

We show that in an identical experimental setup, GLUT3 has 3-fold higher transport affinity and lower turnover than GLUT1, but shows similar substrate selectivity. The 2.4 Å resolution structure of GLUT1 allows us to identify several features, including a glucoside-detergent, NG, found in the central sugar-binding site, several water molecules and a PEG molecule bound to a promiscuous binding-pocket known to be the binding site of endofacial inhibitors (Kapoor et al., 2016). It also reveal two previously unknown features: 1) A chloride-ion binding site, unique for the inward conformation, between the SP and A motifs in the N domain. 2) an intracellular glucose and/or lipid-binding site at the N domain SP motif with a NG molecule bound.

We describe a stabilizing SP-A network that are found in both the N- and C-domains of GLUTs and more generally in Sugar Porter proteins, but only forms in the outward conformation. Our work shows that disruption of the SP-A network destabilizes the outward conformation, and leads to reduced transport affinities. The SP motif acidic residue has a very subtle, but well-defined role in generating this stabilizing SP-A network, and uptake assays confirms significantly increased Km when the glutamate residue of the sugar porter motifs is mutated to neutralize the acidic group.

We find that a chloride ion replaces the acidic position in the inward conformation in the N-domain SP-A network. We propose that this is a general feature of GLUTs and Sugar Porters, and we note that a similar strong peak is observed in the exact same site in the previously published bovine GLUT5 electron density map, which is likely also a Cl^- ion (Nomura et al., 2015).

It has previously been shown that the A motif strongly influences conformational equilibrium, and that manipulations of the A motif results in kinetic changes in Major Facilitators (Sato and Mueckler, 1999; Viitanen et al., 2013; Zhang et al., 2015). The lipid phosphatidylethanolamine (PE) has been suggested to interact with the A motif in other MFS proteins to modulate transport kinetics (Martens et al., 2018). We observe a similar type of interaction here between a glucose or detergent molecule and the SP motif, supporting the idea of endofacial regulation by intracellular modulators.

We further analyzed the GLUT1 C-domain SP motif and identify Lys456 to have a key role in kinetic modulation. By introducing the GLUT1 K456R mutation, mimicking GLUT3, GLUT1 kinetics become GLUT3-like. Conversely, the GLUT3 R454K mutation decrease affinity to similar levels as GLUT1. The conservative modification from Arg to Lys (and vice-versa) show that a precisely tuned interaction network is crucial for transport activity, as previously seen for Major Facilitator motifs (Viitanen et al., 2013).

Based on our results, we suggest a model for kinetic control of the GLUT transport cycle (Fig 6). The A motifs and SP motifs act as molecular switches and together with intracellular modulators control the activation energy between different conformational states, and in particular the rate-

limiting step from empty inward to empty outward conformation. The SP motif glutamate residue has the most prominent role, as this residue forms hydrogen bonds with the A motif backbone residues, creating the SP-A network in the outward conformation to stabilize it. During the transition to the inward conformation, the SP-A network is broken by the glutamate flipping away from the A motif. In this transition, a chloride ion replaces the glutamate residue while an intracellular modulator neutralizes the charged network of the cytosolic residues in the N-domain. This modulator could be a lipid or glucose in a physiological context. This help to stabilize the inward conformation and thus these intracellular modulators indirectly reduce substrate affinity by keeping the transporter in the inward conformation.

It is likely that the N- and C-domain SP-A networks have slightly different properties. While we were able to identify intracellular modulators that interact with the N-domain SP-A network, no such modulators have so far been identified in the C-domain SP-A network. Although we do not exclude the possibility of intracellular modulators playing a role in this network, it is worth noting that the GLUT1 M9 next to the A motif promotes oligomerization (De Zutter et al., 2013). It is possible that GLUT oligomerization could influence the kinetics of transport between monomers in a higher oligomeric state through this interaction.

Our findings suggest that a physiological function of the SP motif is to modulate the kinetics of transport by interacting with the A motif, and function as a structural element that can respond to intracellular modulators such as intracellular glucose levels, lipids and ions. This regulatory function might expand beyond the SP family. We have analyzed the sequences of all known MFS proteins listed in the TCDB database (Saier et al., 2014) and out of the 99 MFS families found in the database (including the SP family), we have identified four additional MFS families that also have an SP sequence motif similar to the one found in the SP family: The Phosphate: H^+ Symporter (PHS) family, the Organic Cation Transporter (OCT) family, the Vesicular Neurotransmitter Transporter (VNT) family and the Plant Copper Uptake Porter (Pl-Cu-UP) family. We predict that these families share elements of the same regulatory mechanism as the SP family.

In conclusion, we have identified molecular switches that modulate glucose transport in GLUTs, and can explain the differences in affinity between GLUT1 and GLUT3. We have presented a model that rationalizes how these switches work, which provides a general function of the SP motif that is the defining feature of the Sugar Porter family. The SP motif is a prime candidate of future work to probe and modify transporter kinetics in both human GLUT transporters as well as more broadly in other SP family members needed for metabolic uptake of sugars in all types of organisms.

Acknowledgements

The authors acknowledge beamlines I24, I04-1 and I04 at the Diamond Light Source, where X-ray data were collected, as well as Max IV Laboratory, DESY-PETRA III and the Swiss Light Source for crystal screening. We also thank H. Nour-Eldin for the pNB1u plasmid backbone used for cloning and oocyte assays. This work was supported by funding from the European Research Council (grant agreement No. 637372), the Novo Nordisk Foundation (grant No. NNF17OC0026900), the Carlsberg Foundation (CF17-0180), an AIAS fellowship to B.P.P. and the Jeppe Juhl and wife Ovita Juhls Memorial Fund to P.A.P.

Author Contributions

T.F.C. did purification and crystallization experiments, collected and processed crystallographic data, yeast complementation assays and oocyte transport assays. P.A.P. did purification and crystallization experiments, collected and processed crystallographic data. B.P.P. supervised the project. T.F.C. and B.P.P. wrote the paper.

Author Information

Coordinates and structure factors have been deposited in the Protein Data Bank with the accession number 6THA. The authors declare no competing interests. Correspondence and requests for materials should be addressed to B.P.P. at bpp@mbg.au.dk.

References

Adams, P.D. *et al.* (2010) 'PHENIX: a comprehensive Python-based system for macromolecular structure solution.', *Acta Crystallogr. D Biol. Crystallogr.* 66, pp. 213–221.

Bailey, T.L. *et al.* (2006), 'MEME: discovering and analyzing DNA and protein sequence motifs.', *Nucleic Acids Res.* 34, pp. W369–W373.

Bentley, P. A. *et al.* (2012) 'Characterization of Bovine Glucose Transporter 1 Kinetics and Substrate Specificities in Xenopus Oocytes', *J Dairy Sci*, 95(3), pp. 1187–1197. doi: 10.3168/jds.2011-4430.

Bond, C.S., Schüttelkopf, A.W. (2009) 'ALINE: a WYSIWYG protein-sequence alignment editor for publication-quality alignments.', *Acta Crystallogr. D Biol. Crystallogr.* 65, pp. 510–512.

Burant, C. F. and Bell, G. I. (1992) 'Mammalian Facilitative Glucose Transporters: Evidence for Similar Substrate Recognition Sites in Functionally Monomeric Proteins', *Biochemistry*, 31(42), pp. 10414–10420. doi: 10.1021/bi00157a032.

Deng, D. *et al.* (2014) 'Crystal structure of the human glucose transporter GLUT1', *Nature*. 510(7503), pp. 121–125. doi: 10.1038/nature13306.

Deng, D. *et al.* (2015) 'Molecular basis of ligand recognition and transport by glucose transporters', *Nature*. 526(7573), pp. 391–396. doi: 10.1038/nature14655.

Ekberg K., *et al.* (2010) 'Structural identification of cation binding pockets in the plasma membrane proton pump', *Proceedings of the National Academy of Sciences*, 107, pp. 21400–21405.

Emsley, P. *et al.* (2010) 'Features and development of Coot', *Acta Crystallographica Section D Biological Crystallography*. 66(4), pp. 486–501. doi: 10.1107/S0907444910007493.

Hresko, R. C. *et al.* (2016) 'Mammalian Glucose Transporter Activity Is Dependent upon Anionic and Conical Phospholipids'. *J Biol Chem.* 291(33):17271-82. doi: 10.1074/jbc.M116.730168.

Iancu, C. V. *et al.* (2013) 'Crystal structure of a glucose/H+ symporter and its mechanism of action', *Proceedings of the National Academy of Sciences*, 110(44), pp. 17862–17867. doi: 10.1073/pnas.1311485110.

Jiang D, *et al.* (2013) 'Structure of the YajR transporter suggests a transport mechanism based on the conserved motif A', *Proceedings of the National Academy of Sciences*, 110, pp. 14664–14669.

Kabsch, W. (2010) 'XDS', *Acta Cryst*, 66, pp. 125–132. doi: 10.1107/S0907444909047337.

Kapoor, K. *et al.* (2016) 'Mechanism of inhibition of human glucose transporter GLUT1 is conserved between cytochalasin B and phenylalanine amides', *Proceedings of the National Academy of Sciences*, 113(17), pp. 4711–4716. doi: 10.1073/pnas.1603735113.

Leduc-Nadeau, A. *et al.* (2007) 'Elaboration of a novel technique for purification of plasma membranes from Xenopus laevis oocytes', *Am J Physiol Cell Physiol*, 292, pp. 1132–1136. doi: 10.1152/ajpcell.00136.2006.-Over.

Lee, E. E. E. *et al.* (2014) 'A Protein Kinase C Phosphorylation Motif in GLUT1 Affects Glucose Transport and is Mutated in GLUT1 Deficiency Syndrome', *Molecular Cell*. 58(5), pp. 845–853. doi: 10.1016/j.molcel.2015.04.015.

Lowe, A. G. and Walmsley, A. R. (1986) 'The kinetics of glucose transport in human red blood cells', *BBA - Biomembranes*, 857(2), pp. 146–154. doi: 10.1016/0005-2736(86)90342-1.

Lyons, J.A. *et al.* (2016) 'Expression strategies for structural studies of eukaryotic membrane proteins', *Curr. Opin. Struct. Biol.* 38, pp. 137–144.

Maher, F., Davies-Hill, T. M. and Simpson, I. A. (1996) 'Substrate specificity and kinetic parameters of GLUT3 in rat cerebellar granule neurons', *Biochem. J.* 315 (Pt 3), pp. 827-31.

Martens, C. et al. (2018) 'Direct protein-lipid interactions shape the conformational landscape of secondary transporters', *Nature Communications*. 9(1), pp. 1–12. doi: 10.1038/s41467-018-06704-1.

McCoy, A. J. *et al.* (2007) 'Phaser crystallographic software', *Journal of Applied Crystallography*. 40(4), pp. 658–674. doi: 10.1107/S0021889807021206.

Mueckler, M. *et al.* (1985) 'Sequence and Structure of a Human Glucose Transporter'. *Science.* 229(4717), pp. 941-5.

Mumberg, D., Müller, R. and Funk, M. (1994) 'Regulatable promoters of Saccharomyces cerevisiae: comparison of transcriptional activity and their use for heterologous expression.', *Nucleic acids research*. 22(25), pp. 5767–8.

Nishimura, H. *et al.* (1993) 'Kinetics of GLUT1 and GLUT4 glucose transporters expressed in Xenopus oocytes', *Journal of Biological Chemistry*, 268(12), pp. 8514–8520.

Nomura, N. *et al.* (2015) 'Structure and mechanism of the mammalian fructose transporter GLUT5', *Nature*. 526(7573), pp. 397–401. doi: 10.1038/nature14909.

Nour-Eldin, H. H., Nørholm, M. H. H. and Halkier, B. A. (2006) 'Screening for plant transporter function by expressing a normalized Arabidopsis full-length cDNA library in Xenopus oocytes', *Plant Methods*, 2(1). doi: 10.1186/1746-4811-2-17.

Oka, Y. *et al.* (1990) 'C-terminal truncated glucose transporter is locked into an inward-facing form without transport activity', *Nature*, 345, pp. 550–553.

Pao, S. S. *et al.* (1998) 'Major facilitator superfamily.', *Microbiology and molecular biology reviews : MMBR*. 62(1), pp. 1–34.

Paulsen, P. A., Custódio, T. F. and Pedersen, B. P. (2019) 'Crystal structure of the plant symporter STP10 illuminates sugar uptake mechanism in monosaccharide transporter superfamily', *Nature Communications*. 10(1), pp. 407. doi: 10.1038/s41467-018-08176-9.

Pei, J., Kim, B.-H., Grishin, N.V. (2008) 'PROMALS3D: a tool for multiple protein sequence and structure alignments.', *Nucleic Acids Res.* 36, pp. 2295–2300.

Quistgaard, E. M. *et al.* (2016) 'Understanding transport by the major facilitator superfamily (MFS): structures pave the way', *Nature Reviews Molecular Cell Biology*, 17(2), pp. 123–132. doi: 10.1038/nrm.2015.25.

Roman, W. *et al.* (1999) 'Concurrent knock-out of at least 20 transporter genes is required to block uptake of hexoses in Saccharomyces cerevisiae', *FEBS letters*. 464(3), pp. 123–128. doi: 10.1016/S0014-5793(99)01698-1.

Saier, M. H. *et al.* (2014) 'The transporter classification database.', *Nucleic acids research*. 42, pp. D251-8. doi: 10.1093/nar/gkt1097.

Sato, M. and Mueckler, M. (1999) 'A conserved amino acid motif (R-X-G-R-R) in the Glut1 glucose transporter is an important determinant of membrane topology', *Journal of Biological Chemistry*, 274(35), pp. 24721–24725. doi: 10.1074/jbc.274.35.24721.

Seyfang, A. and Landfear, S. M. (2000) 'Four conserved cytoplasmic sequence motifs are important for transport function of the Leishmania inositol/H(+) symporter.', *The Journal of biological chemistry*. 275(8), pp. 5687–93. doi: 10.1074/JBC.275.8.5687.

Simpson, I. A. *et al.* (2008) 'The facilitative glucose transporter GLUT3: 20 years of distinction.', *American journal of physiology. Endocrinology and metabolism*. 295(2), pp. E242-53. doi: 10.1152/ajpendo.90388.2008.

Suls, A. *et al.* (2009) 'Early-onset absence epilepsy caused by mutations in the glucose transporter GLUT1', *Annals of Neurology*. 66(3), pp. 415–419. doi: 10.1002/ana.21724.

Sun, L. *et al.* (2012) 'Crystal structure of a bacterial homologue of glucose transporters GLUT1-4', *Nature*. 490(7420), pp. 361–366. doi: 10.1038/nature11524.

Tomasiak, T.M. *et al.* (2014) 'General qPCR and Plate Reader Methods for Rapid Optimization of Membrane Protein Purification and Crystallization Using Thermostability Assays', *Curr. Protoc. Protein Sci.* 77, pp. 29.11.1–14.

Viitanen, P. *et al.* (2013) 'Structure of the YajR transporter suggests a transport mechanism based on the conserved motif A', *Proceedings of the National Academy of Sciences*. 81(6), pp. 1629–1633. doi: 10.1073/pnas.81.6.1629.

Wheeler, T. J., Cole, D. and Hauck, M. A. (1998) ‘Characterization of glucose transport activity reconstituted from heart and other tissues’, *Biochimica et Biophysica Acta*. 1414(1-2), pp. 217-30. doi: 10.1016/s0005-2736(98)00170-9

Winn M.D. *et al.* (2011) ‘Overview of the CCP4 suite and current developments.’, *Acta Crystallogr. D Biol. Crystallogr.* 67, pp. 235–242.

Yan, N. (2015) ‘Structural Biology of the Major Facilitator Superfamily Transporters’, *Annual Review of Biophysics*, (44), pp. 257–283. doi: 10.1146/annurev-biophys-060414-033901.

De Zutter, J. K. *et al.* (2013) ‘Sequence Determinants of GLUT1 Oligomerization Analysis by homology-scanning mutagenesis’, *The journal of biological chemistry*, 288(28), pp. 20734–20744. doi: 10.1074/jbc.M113.469023.

Zhang, X. C. et al. (2015) ‘Energy coupling mechanisms of MFS transporters’, *Protein Science*, 24(10), pp. 1560–1579. doi: 10.1002/pro.2759.

Zhang, X. C. and Han, L. (2016) ‘Uniporter substrate binding and transport: reformulating mechanistic questions’, *Biophysics Reports*. 2(2–4), pp. 45–54. doi: 10.1007/s41048-016-0030-7.

Materials and Methods

Protein expression and membrane isolation

For protein expression in *Saccharomyces cerevisiae,* the GLUT1 gene (UniProt: P11166) followed by a C-terminal purification tag containing a thrombin cleavage site and a deca-histidine tag was cloned into a 2µ expression plasmid, based on p423_GAL1 (Mumberg et al. 1994). Sequence-verified clones were transformed into chemically competent *S. cerevisiae* cells (DSY-5 strain, vendor Gentaur cat# P04003) and plated onto a SD/-His synthetic medium plate and incubated at 30 °C, for 3 days. Freshly grown colonies are inoculated in 10 ml of synthetic medium without histidine, SD-His, (sunrise) and incubatedwith shaking at 180 rpm at 30 ^{o}C. In the following day, the 10 ml culture is inoculated in 1 L of SD/-His synthetic medium overnight and use to grow to high density in a culture-vessel. After harvest, the yeast pellet was re-suspended in Lysis-buffer (100 mM Tris pH 7.5, 600 mM NaCl, 1.2 mM phenylmethylsulfonyl fluoride (PMSF)) and lysed by running 5x1 min cycles on a bead-beating disrupter with 0.5 mm glass beads. The cell-lysate was centrifuged for 20 min at 20.000 g, followed by isolation of membranes by ultracentrifugation at 200.000 g for 150 min. The membranes were homogenized and stored at -80° C.

Protein Purification

Frozen membrane aliquots were thawed on ice and re-suspended in solubilization-buffer (50 mM Tris-HCl pH 7.5, 250 mM NaCl, 5 % glycerol) with 1 % (w/v) n-dodecyl-β-d-maltoside (DDM) and 0.1 % (w/v) Cholesteryl hemisuccinate (CHS)). After incubation for 30 minutes at 4° C, insoluble material was removed by filtration using a 1.2 µm filter. Imidazole to a final concentration of 20 mM was added to the supernatant which was loaded onto a 5 ml Ni-NTA column (GE Healthcare). After loading, the column was washed with 10 column volumes (CV) of W60 buffer (Solubilization buffer with 0.1 % (w/v) DDM, 0.01 % (w/v) CHS and 60mM Imidazole pH 7.5), followed by 10 CV G-buffer (20 mM MES pH 6.5, 250 mM NaCl, 10 % (v/v) Glycerol, 0.2 % (w/v) NG, 0.02 % (w/v) CHS, 0.5 mM tris (2-carboxyethyl) phosphine (TCEP), 40 mM D-glucose). Protein was eluted by circulating G-buffer containing bovine thrombin and 20 mM imidazole at 19 °C for ~16 hours, followed by a 3 CV wash with G-buffer supplemented with 40 mM glucose. The sample was concentrated using a 20 mL concentrator with 100 KDa-cut off (Amicon) and further purified by size exclusion chromatography on an Enrich 650 10/300 column (Bio-rad) in G-buffer. The composition of the G buffer was optimized through a thermostability assay (Tomasiak et al., 2014). Selected peak fractions were pooled and directly used for crystallization trials at ~5 mg/mL. Protein purity was followed through all steps of the purification via SDS gel electrophoresis with InstantBlue Coomassie staining (Expedeon).

Crystallization

Crystals were grown at 17° C by vapor diffusion in 0.6+0.6 µL hanging drops with a reservoir containing 42-46 % polyethylene glycol 400, 100-200 mM $MgCl_2$ and 100 mM Mops pH 7.4. Cubic crystals, with a final size around 100 x 100 x 100 µm, were obtained after 1-3 days of crystal growth. For anomalous experiments to confirm the Cl^- site, crystals were grown using an identical protocol, but exchanging the reservoir solution $MgCl_2$ to $MgBr_2$, before mixing the 0.6+0.6 µL drop.

Data Processing

Data were collected at the Diamond Light Source beamlines i24 and i04, and processed and scaled in space group C2 using XDS (Kabsch, 2010). Complete datasets were obtained from single crystals, but an improved dataset was obtained by averaging data from two separate datasets collected sequentially from a single large crystal. The structures were solved by molecular replacement in PHASER (McCoy et al., 2007) using PDB model 4PYP (Deng et al., 2014). Rfree flags were transferred from 4PYP and extended to the resolution of the dataset. COOT (Emsley et al., 2010) and Namdinator (Kidmose et al., 2019) was used for model building, and refinement was done in phenix.refine (Adams et al., 2010) using a refinement strategy of individual sites, individual ADP and group TLS (3 groups) against a maximum likelihood (ML) target using reflections in the 42-2.4 Å range and yielded an R(work) of 20.4% and R(free) of 22.9%. Residues 1–8 and 456–492 were not visible in density maps and were omitted from the final model. MolProbity (Chen et al., 2010) was used for structure validation and gave a Ramachandran plot with 97.1% of residues in favored regions and 0.2% residues in disallowed regions.

Crystals grown with $MgBr_2$ diffracted to 3.2 Å. Data were collected at the wavelength near the bromine K-absorption edge (0.9184 Å) to maximize the anomalous signal, and after processing a dataset to 4.0 Å in XDS, the anomalous difference Fourier map was calculated using FFT (Acta Cryst. D67, 235-242 (2011)). The map showed one single strong anomalous peak (7.3 sigma) confirming the Cl^- site. Structural figures were prepared using PyMOL 1.5.0.4 (The PyMOL Molecular Graphics System (Schrödinger LLC, 2012)). Sequence alignments were constructed with PROMALS3D (Pei et al., 2008), followed by manually refining gaps based on the observed structure. Alignments were visualized using ALINE (Bond and Schüttelkopf, 2009). SP motifs in the Major Facilitator Superfamily were identified using MEME (Bailey et al., 2009) based on all MFS sequences from TCDB, excluding the SP family (883 sequences total in 98 MFS families, not including SP family sequences) (Saier et al., 2014).

Oocyte transport assays

Human GLUT1 and GLUT3 (UniProt: P11169) were cloned into the pNB1-U vector (Nour-Eldin, Nørholm and Halkier, 2006). All mutations were created using the quick-change lightning site directed mutagenesis kit according to the manufacturer's instructions (Agilent Technologies). The

GLUT3 chimera was generated by amplifying the C-terminal residues 450-492 of GLUT1 and clone them after residue 447 of GLUT3.

525 For cRNA preparation, the genes cloned in the pNB1-U vector were first amplified by PCR using standard primers containing the 5´and 3´UTRs: Fw (TTAACCCTCACTAAAGGGTTGTAATACGACTCACTATAGGG) and Rv (TTTTTTTTTTTTTTTTTTTTTTTTTTTTTATACTCAAGCTAGCCTCGAG), and then analyzed and purified on a 1% agarose gel. RNA was synthesized using the mMESSAGE

530 mMACHINE T7 Transcription Kit (ThermoFisher). Needles for RNA injection were made using the PC-10 Micropipette Puller Narishige. Oocytes from *Xenopus laevis* were purchased from EcoCyte Bioscience (Castrop-Rauxel, Germany). For expression, ~25 ng of RNA were injected into oocytes, using the Nanoject III (Drummond scientific). Prior to uptake assays, oocytes were incubated at 16 ºC for 3 days in ND-96 buffer (82.5 mM NaCl, 2 mM KCl, 1 mM MgCl2, 1 Mm CaCl2, 5 mM HEPES,

535 pH 7.5) with 10 IU/mL streptomycin (Invitrogen). Uptake assays were performed using concentrations of 2-deoxy-D-glucose (Sigma) ranging from 0 to 50 mM in ND-96 buffer. Radioactively labelled deoxyglucose ([3H]-2-DG) was added to each sugar solution at a concentration of 5 µCi/mL (PerkinElmer). In concentration-dependent assays, each group of five oocytes was incubated with the reaction buffer for 30 minutes. The reaction was stopped by adding ice-cold ND-96

540 buffer supplemented with 100 µM Phloretin. For control assays, oocytes were incubated with 20 µM of cytochalasin B in ND-96 buffer for 5 minutes before the uptake assay. In competition assays, the reaction buffer was composed of 5 µCi/mL [3H]-2-DG, 5 mM deoxy-glucose and 20 x fold higher concentration of the competing sugar. Each oocyte was treated as a single experiment. Oocytes were transferred individually to a scintillation vial and disrupted by the addition of 100 µl of a 10 % SDS

545 solution followed by immediate vortexing. 3 ml of EcoScintTM H scintillation fluid (National Diagnostics) was added to each sample and radioactivity was quantified using a Tri-Carb 5110TR Liquid Scintillation Counter (Perkin Elmer). Before analysis, the measured sugar uptake was corrected for unspecific uptake as follows: Water-injected oocytes were exposed to the same 2-DG concentration and time as the GLUT- injected oocytes. This uptake was subtracted before calculating

550 uptake. Experiments were performed at least in triplicates and data was analyzed with Graph Pad Prism 7. Michaelis-Menten fitting was used for curve-fitting analysis and kinetic parameters determination. Error bars represent the standard deviation (SD).

Quantification of protein in oocyte membranes by Western Blot

555 Preparation of total and plasma membrane sections from oocytes was done as described previously (Leduc-Nadeau et al., 2007). For total membranes, five oocytes were rinsed in ND-96 buffer and homogenized in 1 ml of the same solution, supplemented with PMFS (Sigma-Aldrich) by hand with a P200 pipettor. The homogeneous solutions were centrifuged at 16,000 g for 20 min at 4°C to pellet down total membranes. The membrane pellets were resuspended in 10 µl ND-96 buffer with 1 % (v/v)

560 Triton X-100 and frozen until use. For plasma membranes, oocytes were incubated for 10 min in MBSS buffer supplemented with 0.005 % subtilisin A (Sigma-Aldrich) under very mild agitation to partially digest the vitelline membranes. The oocytes were then polymerized at 4°C with 1 % ludox and with 0.1 % polyacrylic acid (Sigma-Aldrich). The oocytes were homogenized by hand with a P200 pipettor in an Eppendorff tube with 0.5 ml of cold HbA (5 mM MgCl2, 5 mM NaH2PO4, 1 mM
565 EDTA, 80 mM sucrose, and 20 mM Tris pH 7.4). The homogenates were diluted to a total volume of 1.5 ml with HbA and centrifuged at 16 g for 30 s at 4°C. This last step was repeated 3 times. Finally, to pellet the purified plasma membranes, the samples were centrifuged at 16.000 g for 20 min.
Prior to western-blotting, proteins from the membrane preparations were separated according to their size by SDS-PAGE gel. Proteins were transfer to a PVDF-membrane (Milipore), using a semi-dry
570 system (Bio-rad). First the PVDF membrane was incubated 60 seconds with 100% of MeOH. The filter paper, membrane and gel were then incubated for 10 min in transfer buffer (25 mM Tris-HCL pH 8.3, 150 mM glycine, 10 % (v/v) methanol). Blotting was performed at room temperature at 18V for 30 min. The PVDF membrane was blocked in 5 % skimmed milk (w/v) in TBS-T (10 mM Tris-HCL pH 8.0, 150 mM NaCl, 0.05 % (w/v) Tween-20 for 1 h at room temperature, with rotation. The
575 membrane was incubate with the primary antibody (anti-GLUT1 Monoclonal antibody, 1:5000) (Abcam) overnight with rotation. The following day, the membrane was washed with TBS-T three times for 10 minutes, prior the incubate with the secondary antibody (α-mouse HRP, 1:1000)(Sigma). The membrane was incubated with the secondary antibody for 1 hour at room temperature, with rotation. The wash was repeated two times and bound antibody was detected using a
580 chemiluminescent substrate solution (Thermo Scientifics).

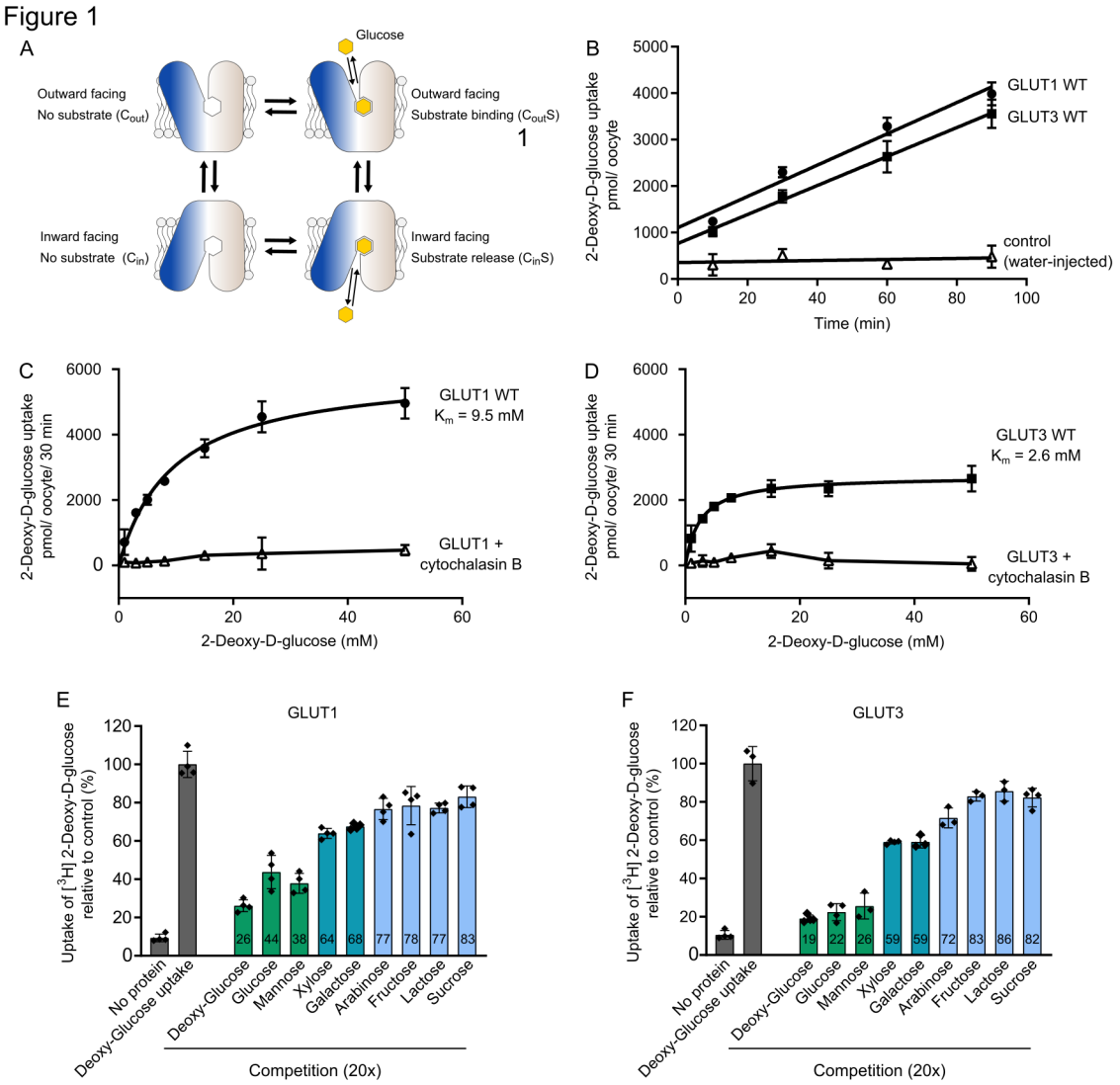

Figure 1. Comparision between GLUT1 and GLUT3

A. Schematic model for transport by GLUTs, alternating between two major conformations with the substrate binding site exposed to the inside and outside of the membrane. Transition between these conformations lead to sugar transport across the membrane following the concentration gradient.

B. Uptake of 2-DG into GLUT1-injected *Xenopus* oocytes (circle) or GLUT3-injected oocytes (squares) or water-injected oocytes (open triangles) at an initial outside concentration of 5 mM 2-DG. For both proteins, 2-DG uptake was linear in the range of 90 minutes. Data for all assays are mean ±SD of three or more replicate experiments.

C. Determination of the kinetic parameters for the transport of 2-DG of GLUT1. The data was fitted using the Michaelis-Menten non-linear fit, yielding a Km = 9.5 ± 1.0 mM and Vmax = 5988 ± 226 pmol/ oocyte/ 30 min. Sugar uptake was inhibited in GLUT1-injected oocytes exposed to cytochalasin B.

D. Determination of the kinetic parameters for the transport of 2-DG of GLUT3. The data was fitted using the Michaelis-Menten non-linear fit, yielding a Km = 2.6 ± 0.4 mM and Vmax = 2731 ± 94 pmol/ oocyte/ 30 min. Sugar uptake was inhibited in GLUT3-injected oocytes exposed to cytochalasin B.

600 E. Substrate selectivity of GLUT1 determined by competition assay in oocytes exposed to 5 mM 2-DG and 20x fold of the competing sugar, for 15 minutes.

F. Substrate selectivity of GLUT3 determined by competition assay in oocytes exposed to 5 mM 2-DG and 20x fold of the competing sugar, for 15 minutes.

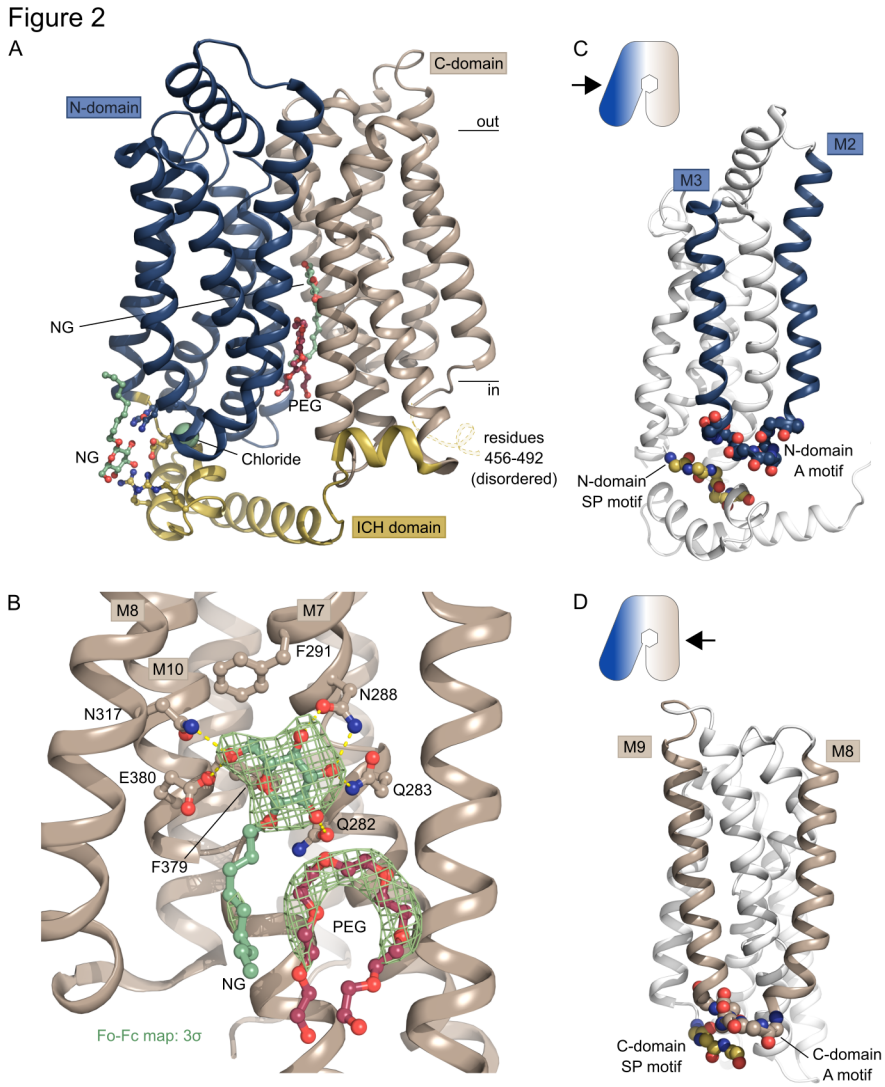

Figure 2. Crystal structure of GLUT1 reveal new ligands

A. The overall structure of GLUT1 in the inward-open conformation. The structure represents a bound state with an NG molecule (shown as sticks) in the central cavity formed between the N-domain (blue) and the C-domain (brown), followed by a PEG molecule (shown as sticks). In close proximity
610 with the ICH domain (yellow) another NG molecule (shown as sticks) was found, as well as a chloride ion (shown as a sphere). Selected residues are shown as sticks. Black bars depict the approximate location of the membrane.

B. Coordination of the glucose moiety in the central cavity by residues from C-domain. Hydrogen bonds are represented by yellow dashes (2.6-3.6 Å distances). The omit Fo-Fc density for NG and
615 PEG is contoured in green at 3σ.

C. Side view of GLUT1 shows the localization of the N-domain SP motif directly underneath the A-motif from the M2-M3 loop. Signature motifs are shown as spheres.

D. Side view of GLUT1 shows the localization of the C-domain SP motif directly underneath the A-motif from the M8-M9 loop. Signature motifs are shown as spheres.

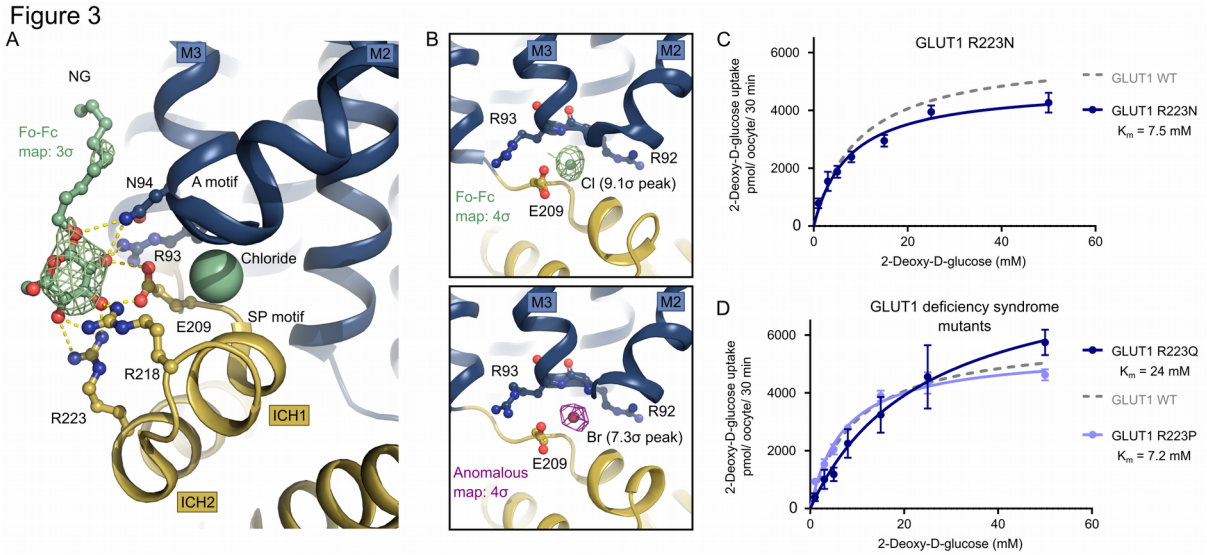

Figure 3. Intracellular molecules stabilize the inward-open conformation

A. Intracellular NG is coordinated by residues from the SP and A motifs. Chloride ion (shown as spheres) neutralizes the A-motif. Hydrogen bonds are represented by yellow dashes (2.6-3.6 Å distances). The omit Fo-Fc density for NG is contoured in green at 3σ.

B. Coordination of the chloride ion by residues of the A-motif. The Fo-Fc electron density, shown in green mesh, is contoured at 4σ (top). The anomalous signal for bromide, shown in magenta mesh, is contoured at 4σ (bottom).

C. Michaelis-Menten analysis of 2-DG uptake of GLUT1 R223N mutant in oocytes. The data was fitted using the Michaelis-Menten non-linear fit, yielding a Km = 7.5 ± 0.8 mM and Vmax = 4838 ± 187 pmol/ oocyte/ 30 min. Data represent the mean ±SD of three or more replicate experiments.

D. Michaelis-Menten analysis of 2-DG uptake of two GLUT1 deficiency syndrome mutants in oocytes. The data was fitted using the Michaelis-Menten non-linear fit, yielding a Km = 7.2 ± 0.6 mM and Vmax = 5436 ± 163 pmol/ oocyte/ 30 min for GLUT1 R223P and Km = 24 ± 4.9 mM and Vmax = 8629 ± 892 pmol/ oocyte/ 30 min for GLUT1 R223Q. Data represent the mean ±SD of three or more replicate experiments.

Figure 4

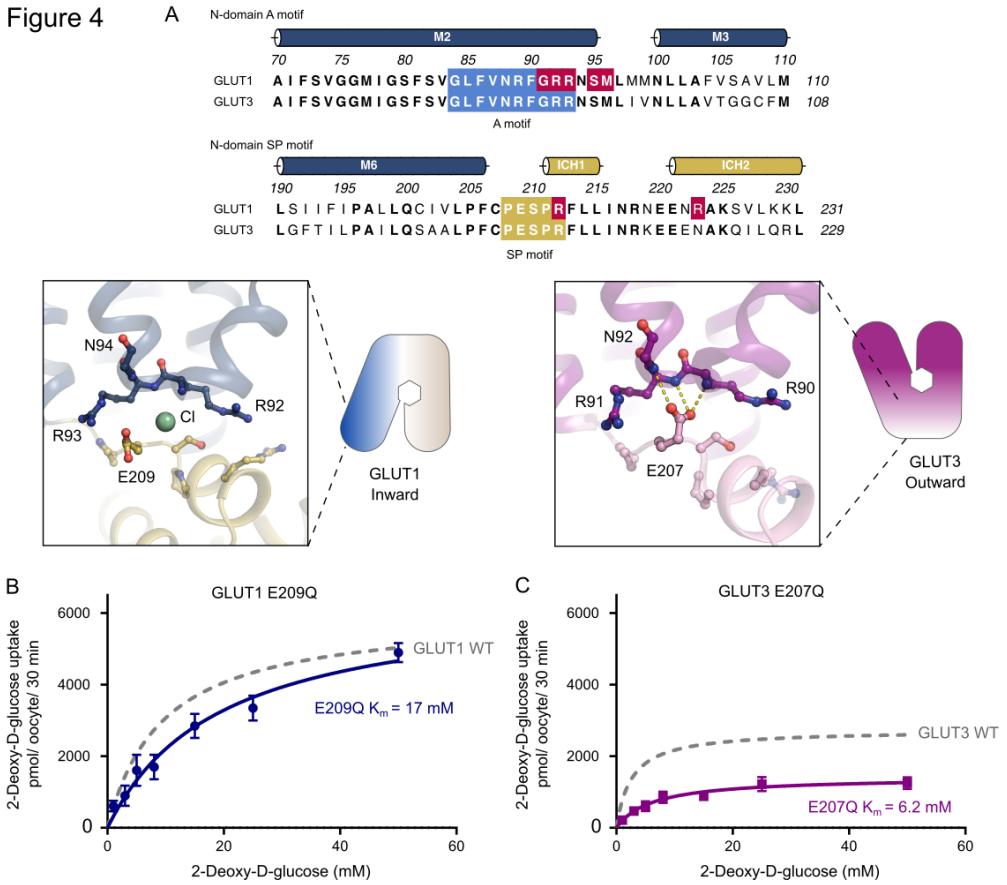

Figure 4. The N-domain SP-A network between transition states

A. Sequence alignment between GLUT1 and GLUT3 of the N-domain A motif (blue) and the N-
640 domain SP motif (yellow). Residues involved in GLUT1 deficiency syndrome are colored in red. N-domain SP-A network in the inward conformation represented by the GLUT1 structure (left) and the outward conformation represented by the GLUT3 structure (PDB 4ZW9) (right). Selected residues are shown as sticks and hydrogen bonds are represented by yellow dashes (2.6-3.6 Å distances).

B-C. Michaelis-Menten analysis of 2-DG uptake in oocytes. Data represent the mean ±SD of three or
645 more replicate experiments. (B) GLUT1 E209Q: Km = 17 ± 3.4 mM and Vmax = 6473 ± 528 pmol/ oocyte/ 30 min. (C) GLUT3 E207Q: Km = 6.2 ± 1.2 mM and Vmax = 1418 ± 88 pmol/ oocyte/ 30 min.

Figure 5

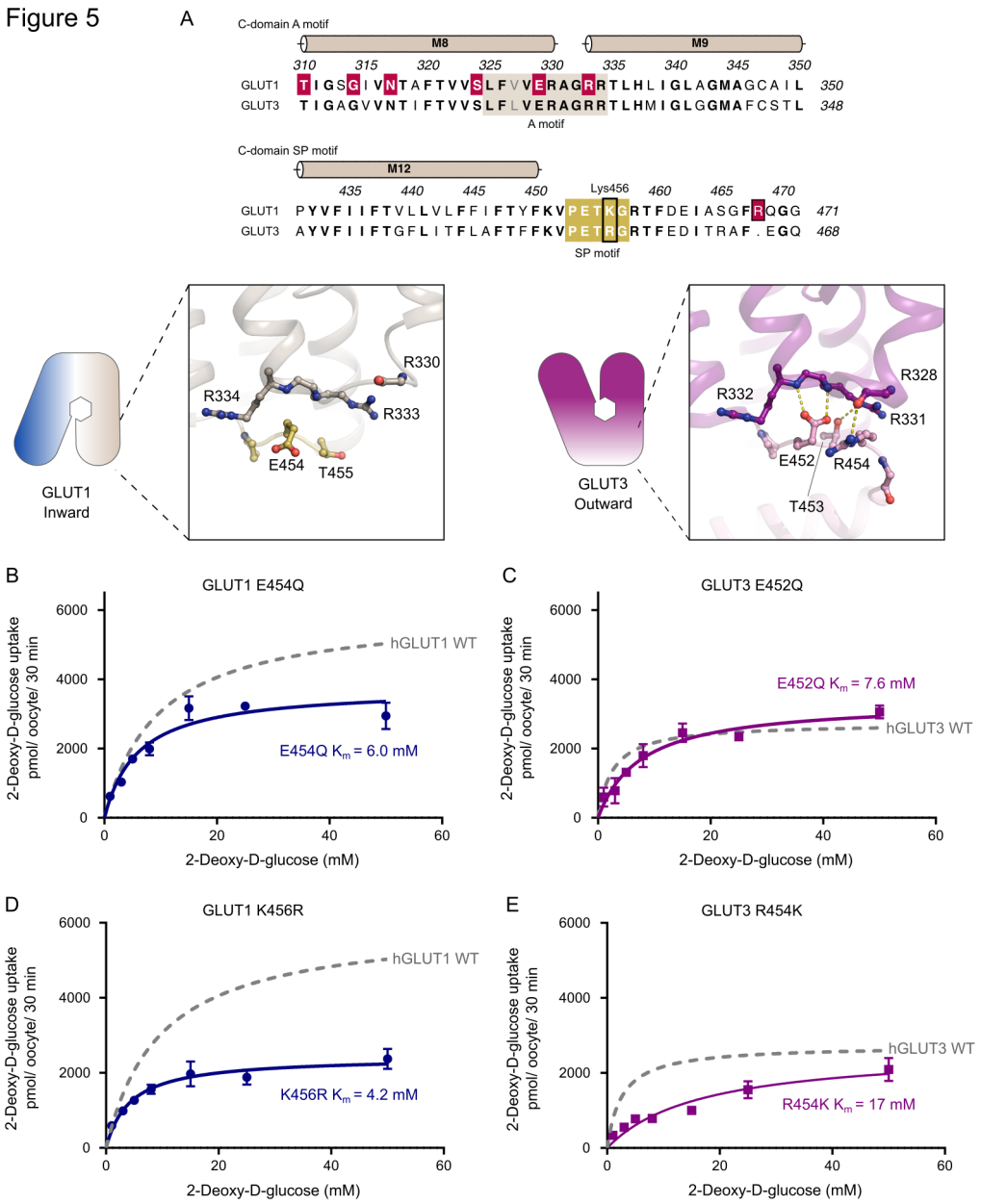

Figure 5 | The C-domain SP-A network between transition states

A. Sequence alignment between GLUT1 and GLUT3 of the C-domain A motif (brown) and the C-domain SP motif (yellow). Residues involved in GLUT1 deficiency syndrome are colored in red. C-domain SP-A network in the inward conformation represented by the GLUT1 structure (left) and the outward conformation represented by the GLUT3 structure (PDB 4ZW9) (right). Selected residues are shown as sticks and hydrogen bonds are represented by yellow dashes (2.6-3.6 Å distances).

B-E. Michaelis-Menten analysis of 2-DG uptake in oocytes. Data represent the mean ±SD of three or more replicate experiments. (B) E454Q: Km = 6.0 ± 1.0 mM and Vmax = 3760 ± 216 pmol/ oocyte/ 30 min. (C) E452Q: Km = 7.6 ± 1.4 mM and Vmax = 3370 ± 204 pmol/ oocyte/ 30 min. (D) K456R: Km = 4.2 ± 0.6 mM and Vmax = 2427 ± 90 pmol/ oocyte/ 30 min. (E) R454K: Km = 17 ± 3.3 mM and Vmax = 2638 ± 234 pmol/ oocyte/ 30 min.

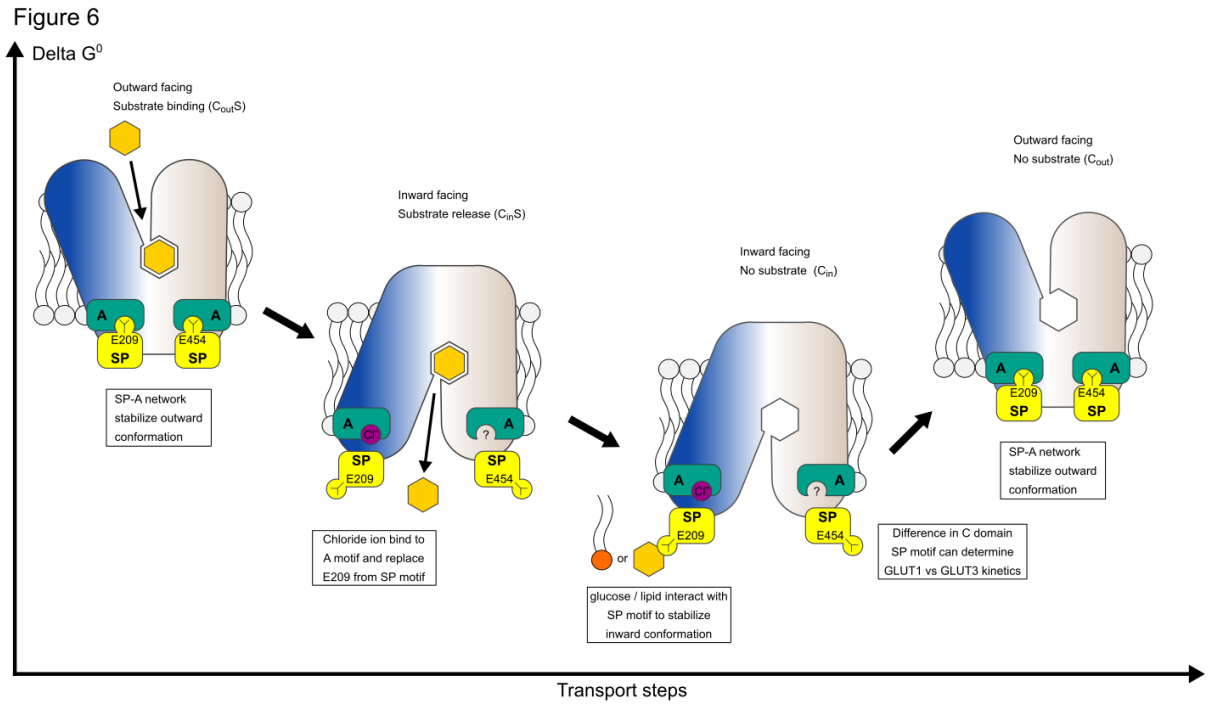

Figure 6. Model for kinetic control of the transport cycle based on the SP-A network.
The SP-A network stabilizes the outward conformation where glucose binds from the extracellular side to the central substrate binding site. Glucose binding leads to closure of the binding site towards
665 the extracellular side and the SP motif glutamate flips away from the A-motif, interchanged by a chloride ion. The disruption of the SP-A network opens the central cavity to the intracellular side and an cytosolic exit pathway for glucose is created. Direct interactions between glucose/lipids with the SP and A motifs stabilize the inward conformation, facilitating the release of glucose.

Supplementary Figures

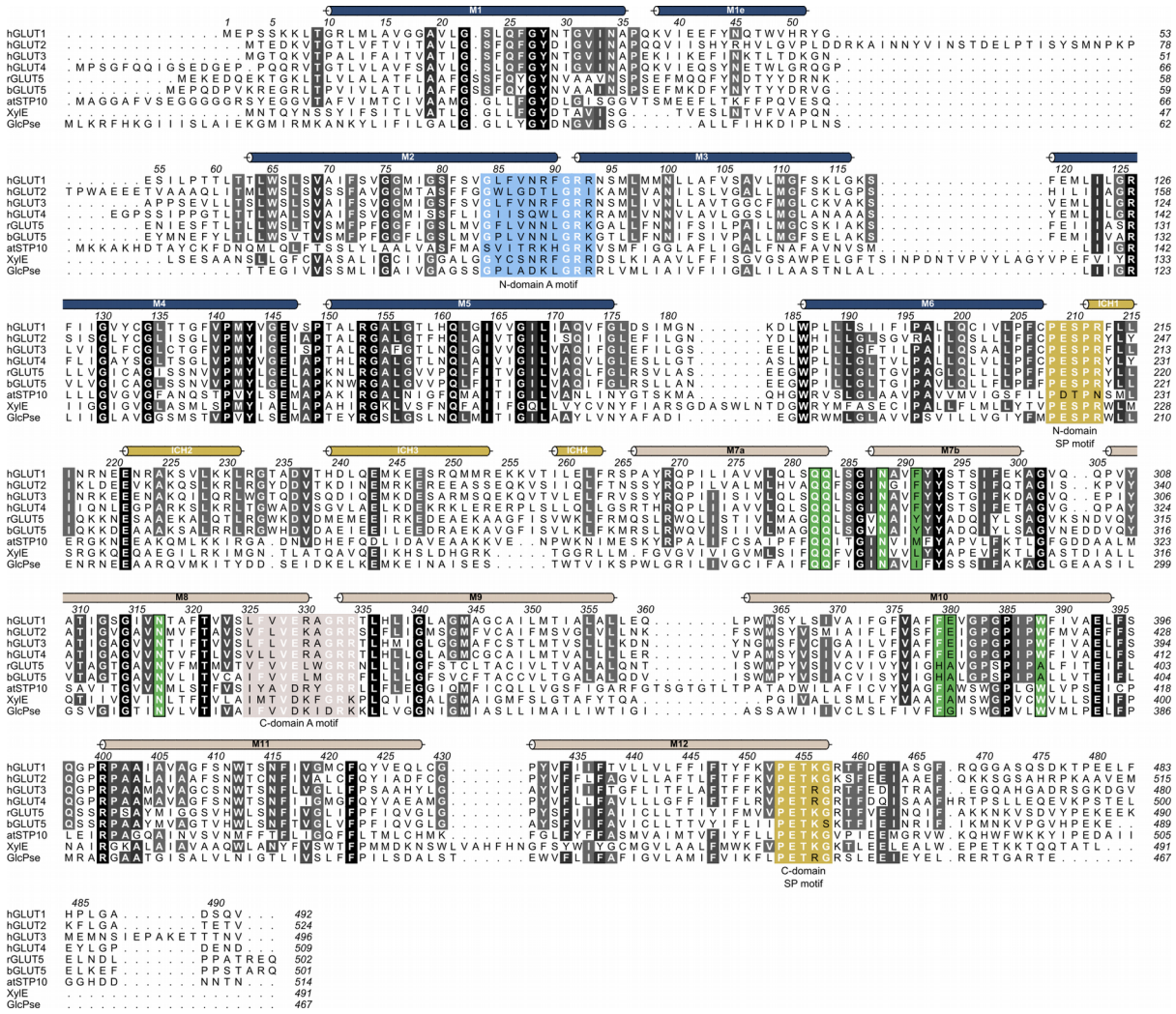

Figure S1. Multiple sequence alignment between human GLUT1 and other structurally characterized members of the Sugar Porter family

Alignment between human GLUT1 (UniProt P11166), GLUT2 (UniProt P11168), GLUT3 (UniProt P11169), GLUT4 (UniProt P14672), rGLUT5 (UniProt P43427), bGLUT5 (UniProt P58353), atSTP10 (UniProt Q9LT15), XylE (UniProt P0AGF4) and GlcPse (UniProt A0A0H2VG78). Conserved residues are highlighted with gray-scale, where black is perfectly conserved. Alpha helices as found in GLUT1 are represented above the sequence as colored tubes. Residues highlighted in blue and brown are the N-domain and C-domain A motifs, respectively. The SP motifs from both domains are highlighted in yellow. In green are residues that create the central substrate binding-site, perfectly conserved between GLUT1-4.

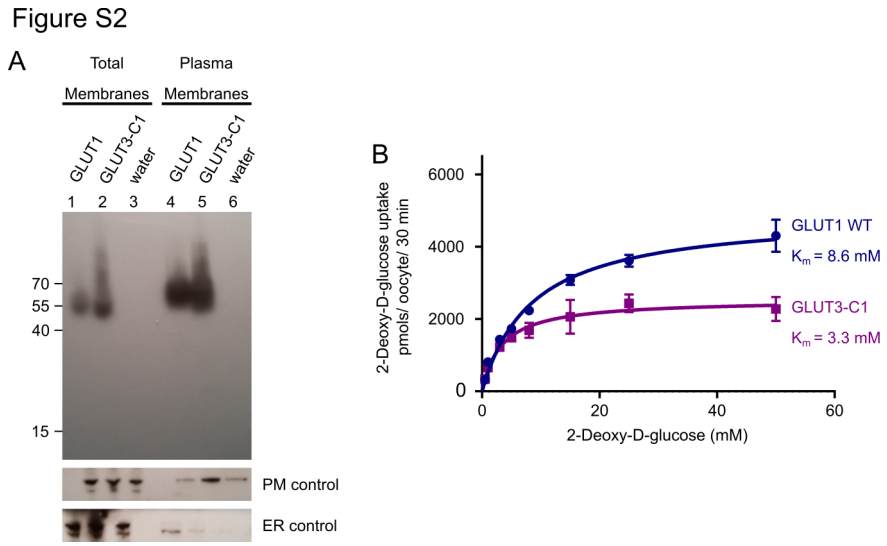

Figure S2. Expression of GLUT1 and GLUT3 chimera in Xenopus oocytes.

A. Western blot analysis between GLUT1-injected oocytes, GLUT3 chimera C1-injected oocytes and water-injected oocytes, from total membrane and plasma membrane preparations. β-integrin is used as a plasma membrane loading control and calnexin as an ER control.

B. Michaelis-Menten analysis of 2-DG uptake between GLUT1 and GLUT3 chimera C1 in *Xenopus* oocytes. The data was fitted using the Michaelis-Menten non-linear fit, yielding a Km = 8.6 ± 0.8 mM and Vmax = 4920 ± 155 pmol/ oocyte/ 30 min for GLUT1 and Km = 3.3 ± 0.5 mM and Vmax = 2537 ± 99 pmol/ oocyte/ 30 min for GLUT3-C1. Data represent the mean ±SD of three or more replicate experiments. Data are mean ±SD of three or more replicate experiments.

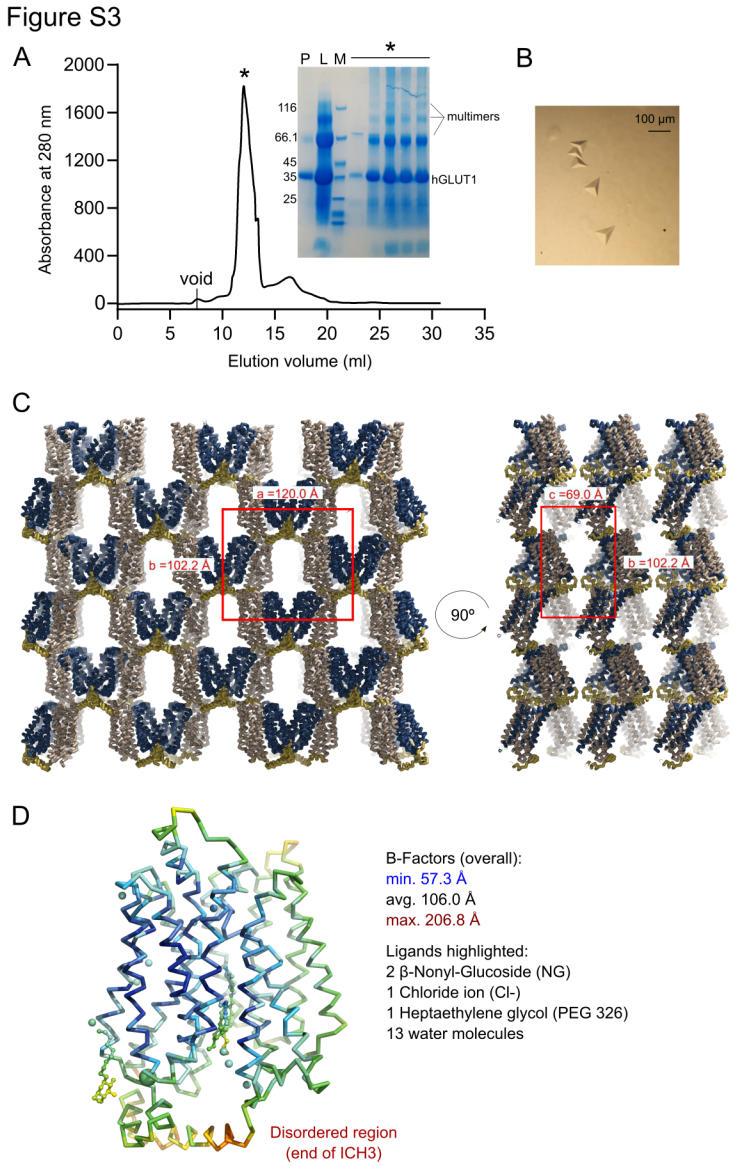

Figure S3. Purification and crystallization of human GLUT1

A. Size exclusion profile of GLUT1 in 0,2 % NG/ 0,02% CHS and the SDS-PAGE correspondent to the protein fraction obtained (P: pool from Ni-NTA; L: SEC load; M: Size marker; *: Peak fractions. Crystal experiments were set up using the peak fractions (~5 mg/ml concentration) directly.

B. GLUT1 crystals.

C. Asymmetric unit and crystal packing of GLUT1. The unit cell is highlighted in red. The asymmetric unit contains one molecule of GLUT1.

D. Backbone representation of GLUT1 and ligands colored by atomic displacement factor (B-factor) with a rainbow gradient from low/blue (57.3 $Å^2$) to high/red (206.8 $Å^2$).

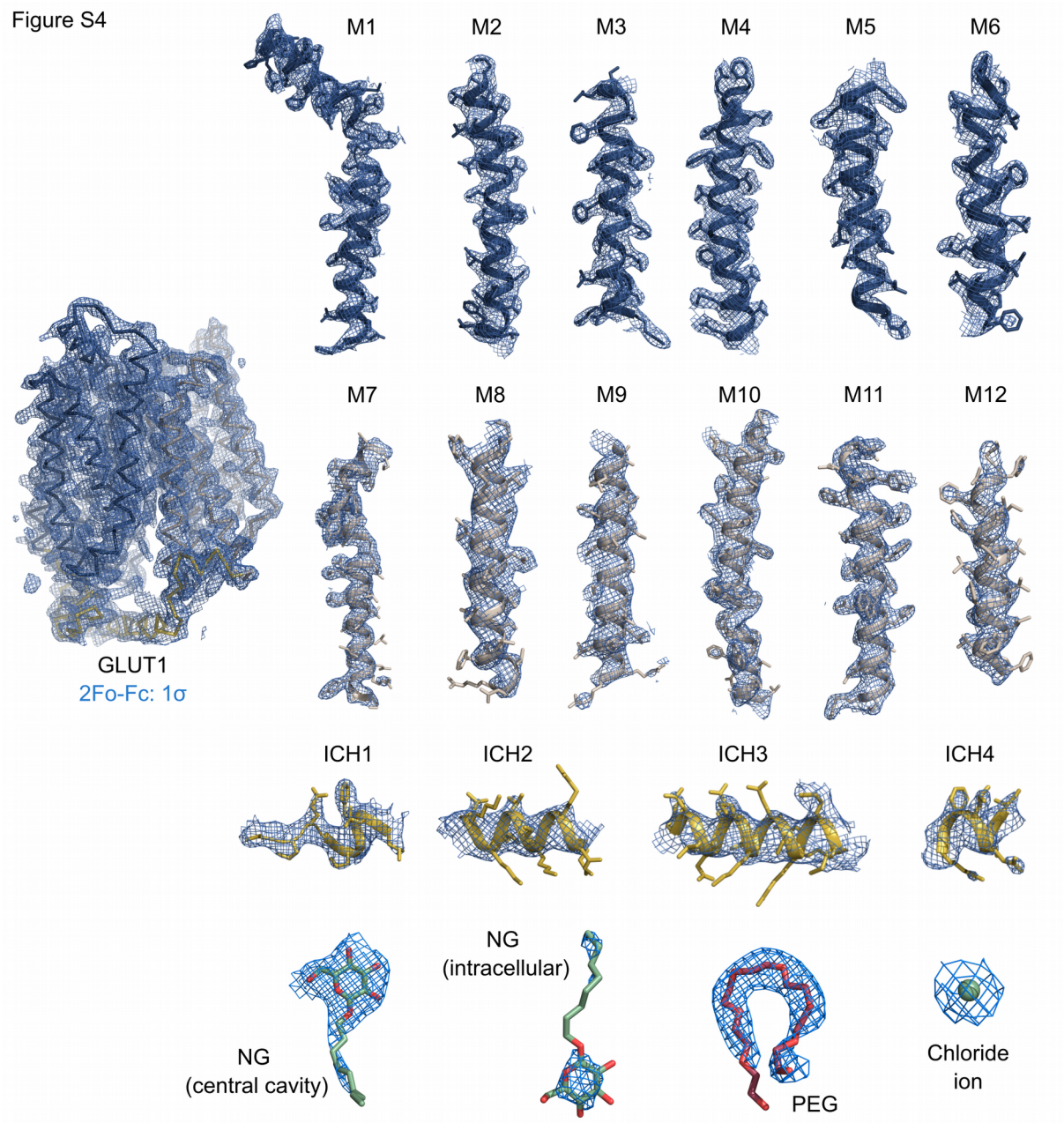

Figure S4. Electron density of the 2.4 Å crystal structure of GLUT1

Weighted 2Fo-Fc electron density map countered at 1.0σ colored in blue with the final model overlaid and amino acid side chains shown as sticks. Maps are shown for individual helices and ligands.

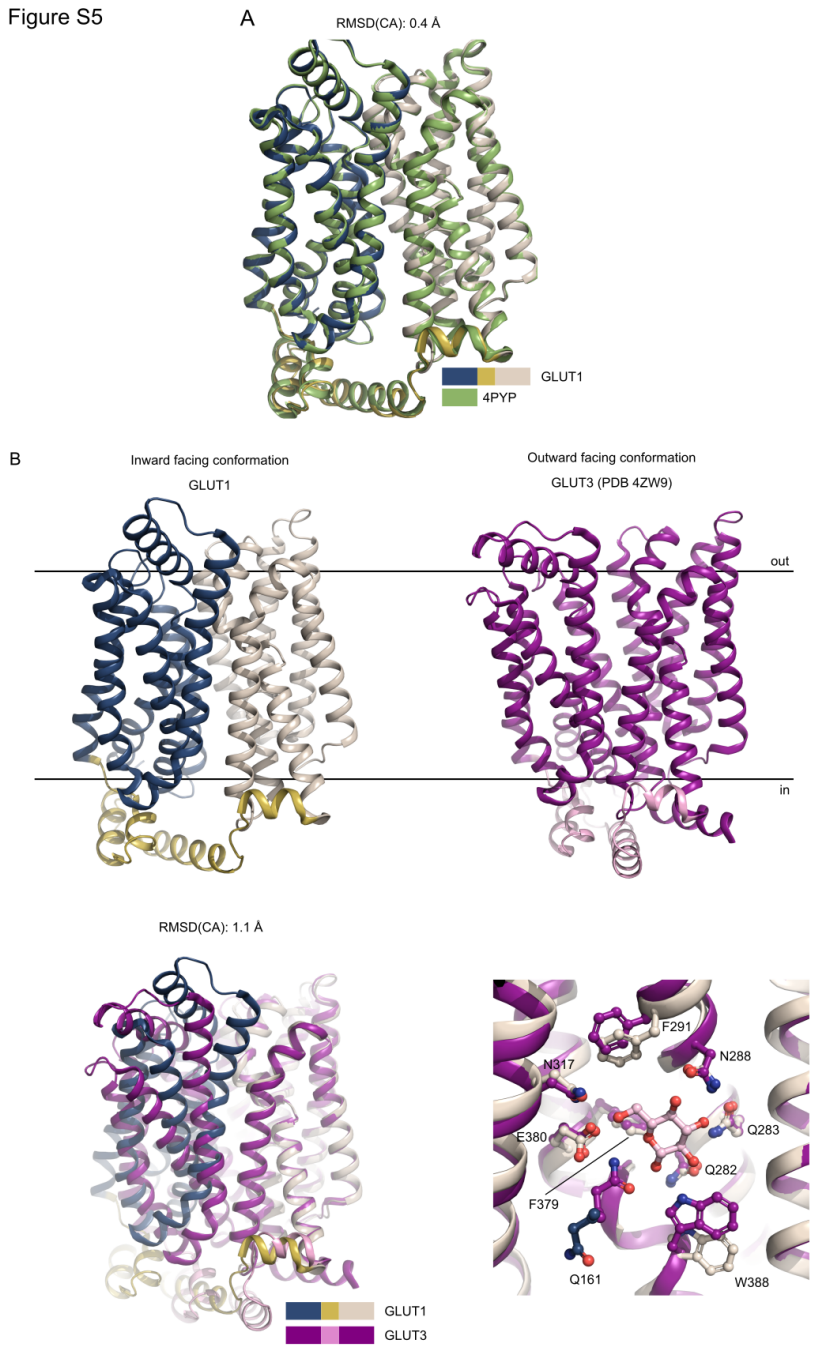

Figure S5. Superposition between GLUTs.

A. Superposition between the GLUT1 (WT, this work, color coded as in Fig. 2) and GLUT1 (N45T/E329Q, PDB 4PYP) show that the models are virtually identical, despite the improved resolution, and the effected of the double mutant is minimal.

B. Comparison between the GLUT1 and the GLUT3 structures. The human GLUT1 structure (this work) was solved in the inward-open conformation, while the GLUT3 structure (PDB 4ZW9) was solved in the outward-open conformation. Superimposition of GLUT1 and GLUT3, relative to their C domains show identical sugar coordination and highlight the movement of the N domain. Residues are labeled according to GLUT1 sequence.

Figure S6

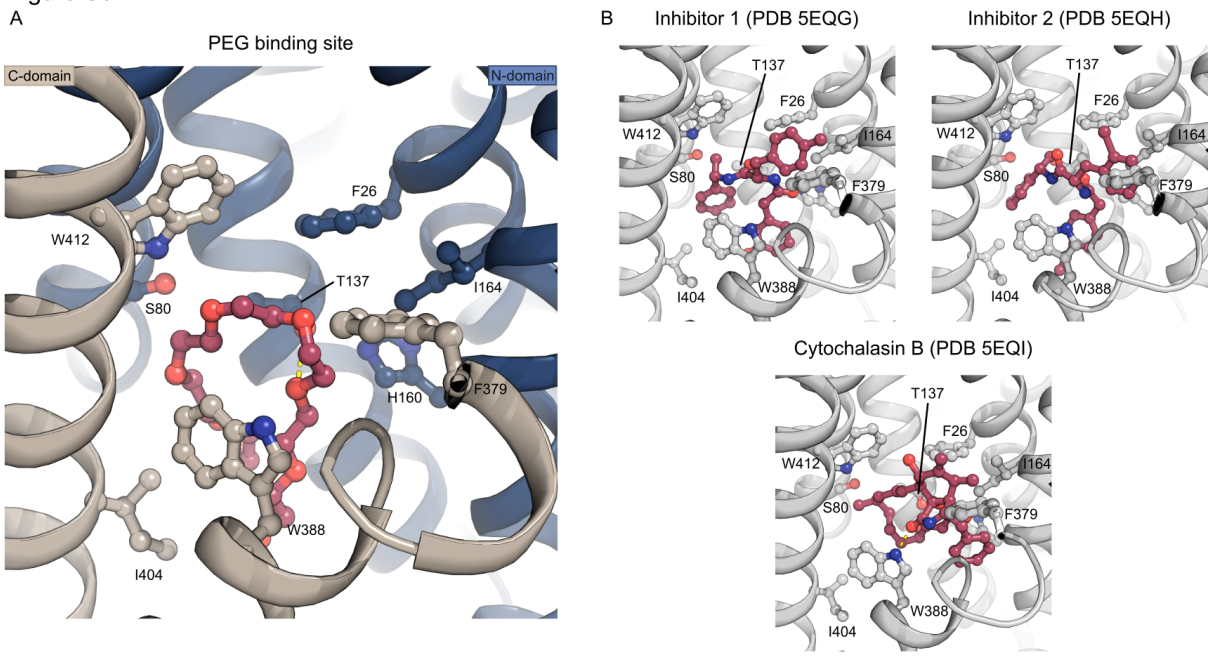

Figure S6. The PEG binding site

A. A PEG molecule (red) was identified just below the central binding-site of glucose, shown as sticks.

B. PEG binding is similar to the binding of endofacial inhibitors 1 (PDB 5EQG) and 2 (PDB 5EQH) previously characterized for GLUT1, while the previously characterized cytochalasin B (PDB 5EQI) binding mode differs. The inhibitors are shown as sticks and colored in red while protein is shown as cartoon and colored in gray.

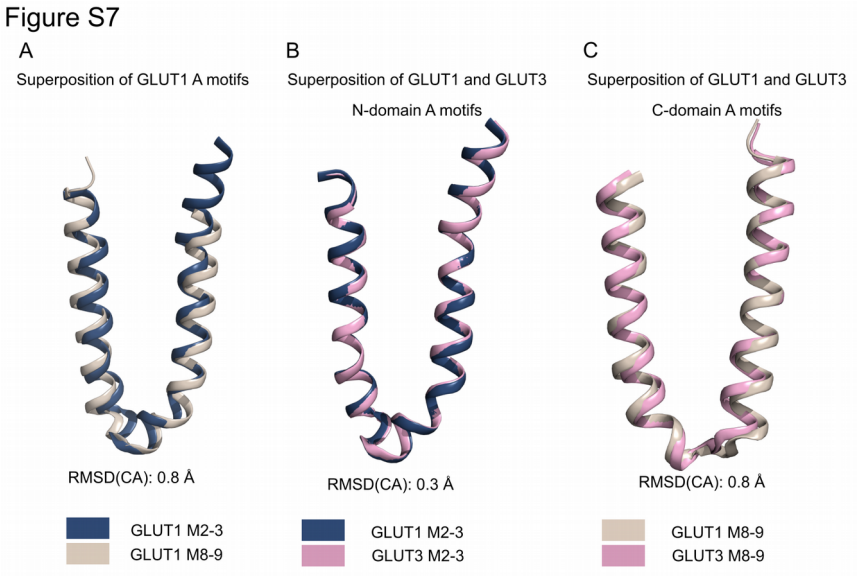

Figure S7. Conservation of the N-domain and C-domain A motifs

A. Superposition of the GLUT1 N-domain A-motif (blue) with the C-domain A-motif (brown), shown as cartoon representation.

B. Superposition of the GLUT1 N-domain A-motif (blue) with the GLUT3 N-domain A-motif (pink), shown as cartoon representation.

C. Superposition of the GLUT1 C-domain A-motif (brown) with the GLUT3 C-domain A-motif (pink), shown as cartoon representation.

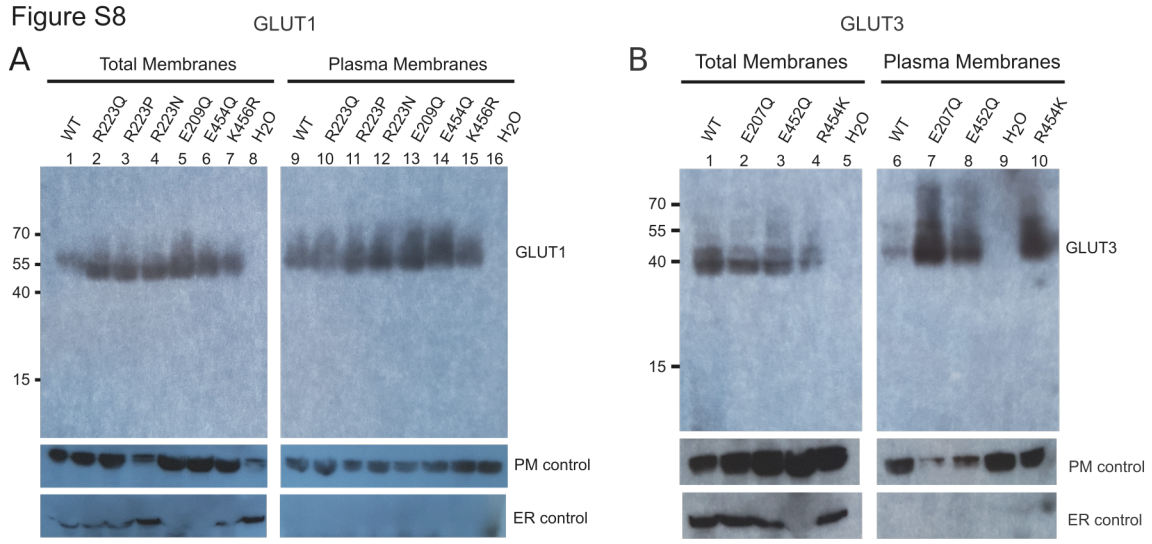

Figure S8. Expression of GLUT mutants in Xenopus oocytes

A. Western blot analysis between GLUT1-injected oocytes, GLUT1 mutants and water-injected oocytes, from total membrane and plasma membrane preparations. β-integrin is used as a plasma membrane loading control and calnexin as an ER control.

B. Western blot analysis between GLUT3-injected oocytes, GLUT3 mutants and water-injected oocytes, from total membrane and plasma membrane preparations. β-integrin is used as a plasma membrane loading control and calnexin as an ER control.

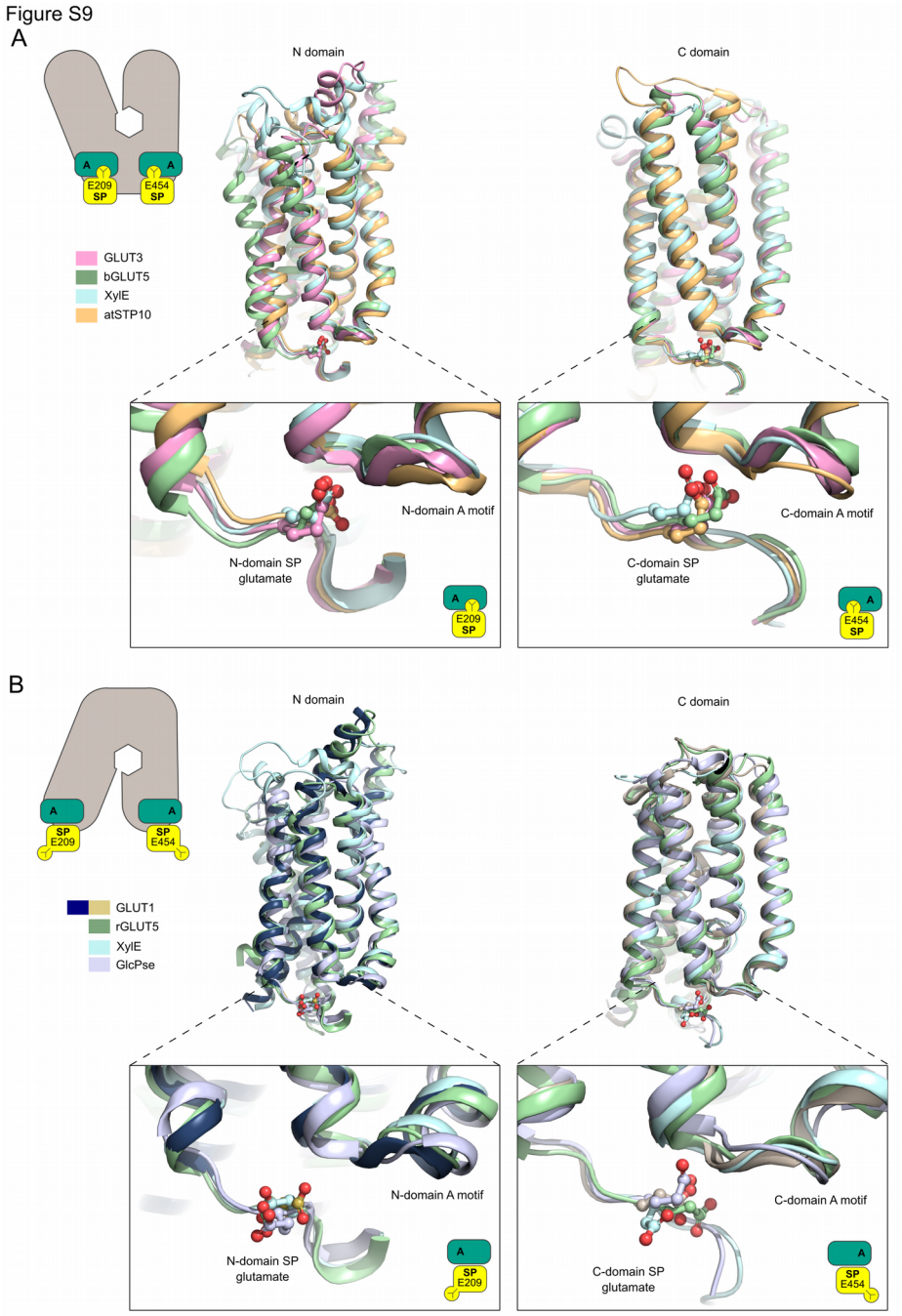

Figure S9. The SP motif glutamate residue in known SP proteins structures

A. Outward-open conformation structures from GLUT3 (pdb 4ZW9), rGLUT5 (pdb 4YBQ) and atSTP10 (pdb 6H7D) were superimposed relative to their N domains (left) or C domains (right). The glutamate residues (shown as sticks) in both N (bottom left) and C (bottom right) domains motifs are pointing towards the A-motif.

B. Inward-open conformation structures from GLUT1 (this work), the GlcPse (pdb 4LDS) and bGLUT5 (pdb 4YB9) were superimposed relative to their N domains (left) or C domains (right). The glutamate residues (shown as sticks) in both N (bottom left) and C domains (bottom right) motifs are pointing away from the A motif, with the exception of the C domain glutamate of the GlcPse (bottom right).

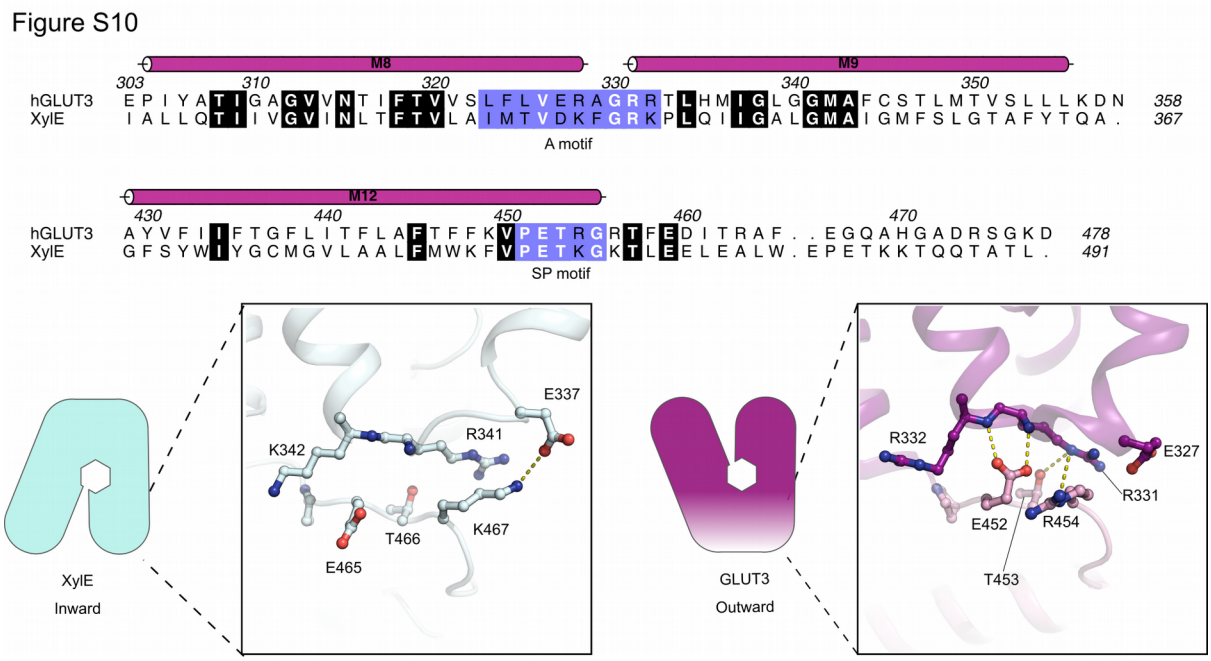

Figure S10. The N-domain SP-A network of the GLUT1 bacterial homologue

755 Sequence alignment between GLUT3 (UniProt P11169) and XylE (UniProt P0AGF4) of the C-domain A motif and the C-domain SP motif. Conserved residues are highlighted in bold. The residues belonging to the A motif and the SP motif are colored in blue. C-domain SP-A network in the inward conformation represented by the XyLE structure (PDB 4JA4) (left) and the outward conformation represented by the GLUT3 structure (PDB 4ZW9) (right). Selected residues are shown as sticks and

760 hydrogen bonds are represented by yellow dashes (2.6-3.6 Å distances).

Table S1. Statistics for Crystallographic Data Collection and Structure Refinement.

Name	**hGLUT1**	**hGLUT1**
Type	native	bromide
Data Collection		
Space group	C2	C2
Cell dimensions		
a. b, c (Å)	120.0, 102.2, 69.0	119.4, 102.7, 67.2
alpha, beta, gamma (deg)	90.0, 98.9, 90.0	90.0, 99.9, 90.0
Monomers per asym. unit.	1	1
Wavelenght (Å)	0.9686	0.9188
Number of reflections measured	229827	35341
Number of unique reflections	32166	13041
Resolution (Å)	48-2.4 (2.5-2.4)[a]	77-4.0 (4.1-4.0)[a]
Rmeas (%)	12.3 (238.0)	7.1 (20.8)
Mean I/σ(I)	7.2 (0.7)	12.7 (6.4)
CC(1/2)	99.8 (44.4)	99.8 (54.3)
Completeness (%)	99.9 (100.0)	97.9 (96.6)
Redundancy	7.1 (7.6)	2.7 (2.7)
Refinement		
Resolution (Å)	41.7-2.4 (2.48-2.40)	
No. reflections (work/free)	32117/3161	
Rwork (%)	20.44	
Rfree (%)	22.94	
No. of Atoms		
Protein	3478	
Ligands	65	
Waters	13	
Average B Factors (Å)		
Overall	106.0	
Protein	105.9	
Ligands	114.1	
Waters	91.8	
RMSD		
Bond lenghts (Å)	0.004	
Bond angles (deg)	0.65	
Ramachandran Plot Statistics		
Favored regions	97.1	
Allowed regions	2.7	
Disallowed regions	0.2	
Deposited model (PDB id)	6THA	

[a]Highest resolution shell is shown in parenthesis.

Table S1. Data collection and refinement statistics